

AN ADAPTIVE INCLINED 3D PRINTER FOR MINIMUM SUPPORT  
STRUCTURE GENERATION IN FUSED FILAMENT FABRICATION PROCESS

A THESIS SUBMITTED TO  
THE GRADUATE SCHOOL OF NATURAL AND APPLIED SCIENCES  
OF  
MIDDLE EAST TECHNICAL UNIVERSITY

BY

HAKAN DOĞAN

IN PARTIAL FULFILLMENT OF THE REQUIREMENTS  
FOR  
THE DEGREE OF MASTER OF SCIENCE  
IN  
MECHANICAL ENGINEERING

NOVEMBER 2022



Approval of the thesis:

**AN ADAPTIVE INCLINED 3D PRINTER FOR MINIMUM SUPPORT  
STRUCTURE GENERATION IN FUSED FILAMENT FABRICATION  
PROCESS**

submitted by **HAKAN DOĞAN** in partial fulfillment of the requirements for the degree of **Master of Science in Mechanical Engineering Department, Middle East Technical University** by,

Prof. Dr. Halil Kalıpçılar  
Dean, Graduate School of **Natural and Applied Sciences** \_\_\_\_\_

Prof. Dr. M. A. Sahir Arıkan  
Head of Department, **Mechanical Engineering** \_\_\_\_\_

Assoc. Prof. Dr. Ulaş Yaman  
Supervisor, **Mechanical Engineering, METU** \_\_\_\_\_

**Examining Committee Members:**

Prof. Dr. Melik Dölen  
Mechanical Engineering, METU \_\_\_\_\_

Assoc. Prof. Dr. Ulaş Yaman  
Mechanical Engineering, METU \_\_\_\_\_

Assoc. Prof. Dr. Sezer Özerinç  
Mechanical Engineering, METU \_\_\_\_\_

Assoc. Prof. Dr. Yusuf Sahillioğlu  
Computer Engineering, METU \_\_\_\_\_

Prof. Dr. Oğuzhan Yılmaz  
Mechanical Engineering, Gazi University \_\_\_\_\_

Date: 24.11.2022



**I hereby declare that all information in this document has been obtained and presented in accordance with academic rules and ethical conduct. I also declare that, as required by these rules and conduct, I have fully cited and referenced all material and results that are not original to this work.**

Name, Surname: Hakan Dođan

Signature :

## **ABSTRACT**

### **AN ADAPTIVE INCLINED 3D PRINTER FOR MINIMUM SUPPORT STRUCTURE GENERATION IN FUSED FILAMENT FABRICATION PROCESS**

Dođan, Hakan

M.S., Department of Mechanical Engineering

Supervisor: Assoc. Prof. Dr. Ulař Yaman

November 2022, 77 pages

After the expiration of the patent on the Fused Filament Fabrication (FFF) type of additive manufacturing method, people have started various technological companies to improve the process and its fundamental equipment. One of these advancements was on the slicing plane orientation of the FFF 3D printers. Instead of having the conventional horizontal slicing planes, few companies developed similar 3D printers capable of extruding material at a fixed angle of inclination. Another great advantage of their configuration is that the printer has an infinite building volume, which enables mass production with the FFF process. The problem with this approach is that the inclination angle of the 3D printer is fixed and it may be inefficient for the fabrication of various parts. In this study, a novel slicing methodology is implemented using Rhino3D (CAD software) and Grasshopper3D (analytical modeling tool for Rhino3D) environments with adaptive slicing planes. Later, a conveyor belt is integrated onto a multi-axis 3D printer to realize the proposed approach. Several parts are fabricated and the advantages of the method are elaborated over these example artifacts.

Keywords: Additive Manufacturing, 3D Printing, Inclined Slicing, FFF, Adaptive, Support Structures



## ÖZ

### **ERGİYİK FİLAMANT İLE İMALAT İŞLEMİNDE EN AZ DESTEK YAPISI KULLANIMI İÇİN ADAPTİF VE EĞİMLİ 3 BOYUTLU YAZICI SİSTEMİ**

Doğan, Hakan

Yüksek Lisans, Makina Mühendisliği Bölümü

Tez Yöneticisi: Doç. Dr. Ulaş Yaman

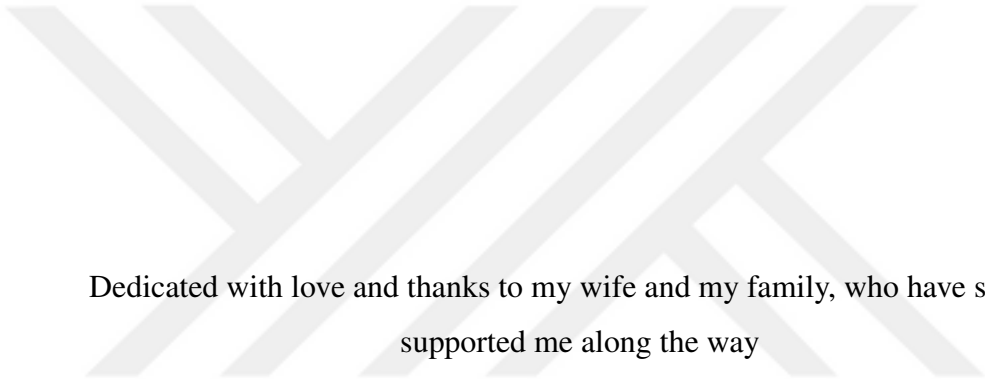
Kasım 2022 , 77 sayfa

Ekllemeli imalatta en sık kullanılan yöntem olan Ergiyik Filament ile İmalat (Fused Filament Fabrication, FFF) patentinin sona ermesiyle birlikte, birçok şirket ve araştırmacı bu teknolojiyi geliştirmeye ve ilerletmeye başlamıştır. Bu gelişmelerden biri de FFF 3B yazıcılar için dilimleme düzleminin belirlenmesi ile ilgilidir. Alışılmamış olan yatay dilimlerin aksine, farklı şirketler ekstrüder sistemini 45° eğime sahip olan bir düzlem üzerine kurmuşlardır. Bu şekilde hem gerekli destek malzeme miktarı azalmış, hem de bir taşıma bandıyla toplu üretim ve sonsuz uzunlukta parçaların üretilebilmesi mümkün olmuştur. Oldukça verimli bir yaklaşım olan bu yöntemde, imalat düzlemi eğik ve sabit bir açıda tutulmaktadır. Bu açının, sunulan geometrinin çeşitli kısımlarına göre adaptif bir şekilde değişebilmesi, daha etkili bir üretim imkanı sunacaktır. Bu çalışmanın temelinde, özgün bir yaklaşımla Rhino 3D (Bilgisayar Destekli Tasarım yazılımı) ve Grasshopper 3D (Rhino 3D için analitik modelleme aracı) kullanılarak bir dilimleme algoritması geliştirilmiştir. Daha sonrasında bir taşıma bandı çok eksenli 3B bir yazıcıya bağlanarak yöntemin uygulaması gerçekleştirilmiştir. Farklı parçalar üretilmiş ve yöntemin avantajları örnekler üzerinden

açıklanmıştır.

Anahtar Kelimeler: Eklemeli İmalat, 3B Yazıcı, Eğimli Dilimleme, FFF, Adaptif, Destek Yapıları





Dedicated with love and thanks to my wife and my family, who have strongly supported me along the way

## ACKNOWLEDGMENTS

The start of this thesis study coincided with the COVID-19 Global Pandemic. Those were hard times, so first of all, I would like to express my deepest appreciation to my Supervisor, Assoc. Dr. Ulaş Yaman, who consistently and patiently supported me throughout the study despite any difficulties.

I would also like to deeply thank to Uğur Mecid Dilberođlu and Eyüp Furkan Peköz for their work during the production and integration stage of the algorithm.

Finally, special thanks to my wife, Dilmin Dođan. Our marriage also coincided with the start of the study and she supported me strongly along the way. Also, special thanks to my whole family for their belief, and my friends Ertuđrul ubuk & Őükrü Bezen for their support.

## TABLE OF CONTENTS

ABSTRACT . . . . .	v
ÖZ . . . . .	vii
ACKNOWLEDGMENTS . . . . .	x
TABLE OF CONTENTS . . . . .	xi
LIST OF FIGURES . . . . .	xiv
LIST OF ABBREVIATIONS . . . . .	xviii
CHAPTERS	
1 INTRODUCTION . . . . .	1
1.1 Motivation and Problem Definition . . . . .	1
1.2 Proposed Methods and Models . . . . .	2
1.3 Contributions and Novelties . . . . .	2
1.4 The Outline of the Thesis . . . . .	3
2 BACKGROUND . . . . .	5
2.1 Introduction . . . . .	5
2.2 Additive Manufacturing . . . . .	5
2.3 Fused Filament Fabrication . . . . .	6
2.3.1 Parameters in Fused Filament Fabrication . . . . .	7
2.4 Generation of Support Structures . . . . .	8

2.4.1	Object Partitioning . . . . .	9
2.4.2	Inclination . . . . .	10
2.4.3	Shape & Support Modification . . . . .	11
2.4.4	Multi-Axis Additive Manufacturing . . . . .	13
2.5	Design for Additive Manufacturing . . . . .	15
2.6	Continuous 3D Printing & Mass Production with Additive Manufacturing . . . . .	15
3	ADAPTIVE INCLINED SLICING ALGORITHM . . . . .	21
3.1	Introduction . . . . .	21
3.2	Tree Structure & Flowchart . . . . .	22
3.2.1	Tree Structure . . . . .	22
3.2.2	Flowchart . . . . .	24
3.3	Inputs . . . . .	27
3.4	Slicing . . . . .	28
3.4.1	Initial Movement & Projection . . . . .	29
3.5	Support Derivation & Optimization . . . . .	35
3.5.1	Object Partition . . . . .	35
3.5.2	Support Structures . . . . .	37
3.6	Shell & Infill Patterns . . . . .	40
3.7	Manufacturing Data . . . . .	43
3.8	Sample Geometries . . . . .	44
3.8.1	Square Collar . . . . .	44
3.8.2	Hanger . . . . .	47

3.9	Time Complexity Analysis . . . . .	49
4	FABRICATION OF SAMPLE ARTIFACTS . . . . .	51
4.1	Introduction . . . . .	51
4.2	Hardware . . . . .	51
4.3	Integration onto the Multi-axis Manufacturing System . . . . .	54
4.4	Test Prints . . . . .	59
4.4.1	Sample 1 - Single Angle . . . . .	59
4.4.2	Sample 2 - Double Angle . . . . .	61
4.4.3	Sample 3 - Triple Angles . . . . .	65
5	CONCLUSIONS . . . . .	69
	REFERENCES . . . . .	71
	APPENDICES	
A	GHPYTHON SCRIPTS . . . . .	75
A.1	Slicing Angle Derivation . . . . .	75
A.2	Manufacturing Data Generation . . . . .	76

## LIST OF FIGURES

### FIGURES

Figure 2.1	A Standard Fused Filament Fabrication Setup [6] . . . . .	6
Figure 2.2	Sample Cases for Overhanging and Bridging Support Requirements [7]. . . . .	8
Figure 2.3	Object partitioning sample, the sub-parts assembled to eliminate the support structure requirement [9]. . . . .	9
Figure 2.4	Comparison of inclined and conventional FFF processes. . . . .	10
Figure 2.5	Inclined layer printing process [13] . . . . .	11
Figure 2.6	Support volume reduction by modification [15] . . . . .	12
Figure 2.7	Support volume reducing by modification [17] . . . . .	13
Figure 2.8	Multi-axis AM with a moving printer bed [18] . . . . .	14
Figure 2.9	Multi-Axis 3D printer with multiple nozzles [19] . . . . .	14
Figure 2.10	Volume limitations of various 3D printers. [23] . . . . .	16
Figure 2.11	Koala 3D, a continuous climbing 3D printer [25] . . . . .	17
Figure 2.12	Inclined 3D printer with a conveyor belt, BlackBelt 3D [27] . . . . .	18
Figure 2.13	Inclined 3D printer with a conveyor belt, Creality CR-30 [28]. . . . .	19
Figure 3.1	Example tree path for {0;7;1;3} . . . . .	23
Figure 3.2	Process flowchart . . . . .	24

Figure 3.3	Flowchart of the orientation computation . . . . .	25
Figure 3.4	Flowchart of the least support optimization . . . . .	26
Figure 3.5	The Stanford Bunny, low poly version. . . . .	28
Figure 3.6	The Stanford Bunny, sample orientation . . . . .	29
Figure 3.7	Angle sectors and conditions . . . . .	30
Figure 3.8	Example Process for Slicing . . . . .	32
Figure 3.9	Green: Projection   Blue: Outward Normals   Red: Slicing Planes . . . . .	34
Figure 3.10	Green: Projection   Blue: Outward Normals   Red: Slicing Planes . . . . .	34
Figure 3.11	The Stanford Bunny, divided . . . . .	35
Figure 3.12	The Stanford Bunny, intersected . . . . .	36
Figure 3.13	Stanford Bunny, Divided, Extruded . . . . .	37
Figure 3.14	The Stanford Bunny, constructed with overhanging support vol- umes. . . . .	38
Figure 3.15	The green part is used to carry the cyan support volume. . . . .	39
Figure 3.16	Representations of the nozzle diameter, shells & infill patterns. . . . .	40
Figure 3.17	Representation of Nozzle Path, Shells & Infill, Single Layer . . . . .	41
Figure 3.18	Representation of Nozzle Path, Shells & Infill, Single Layer, Islands . . . . .	41
Figure 3.19	Representation of Nozzle Path, Shells & Infill, Complete Geometry . . . . .	42
Figure 3.20	Square Collar . . . . .	44
Figure 3.21	Square Collar Slicing, Normal View . . . . .	45

Figure 3.22	Square Collar Slicing, Perspective . . . . .	46
Figure 3.23	Square Collar, Rendered . . . . .	46
Figure 3.24	Hanger, Sample . . . . .	47
Figure 3.25	Hanger Slicing, Perspective . . . . .	47
Figure 3.26	Hanger Slicing, Normal View . . . . .	48
Figure 3.27	Hanger, Rendered . . . . .	48
Figure 4.1	Multi-axis 3D printer [32] . . . . .	52
Figure 4.2	Conveyor Belt Model, Rendered . . . . .	52
Figure 4.3	Conveyor belt . . . . .	53
Figure 4.4	Conveyor belt assembly . . . . .	53
Figure 4.5	Setup for Sample 1 . . . . .	59
Figure 4.6	Sample 1 . . . . .	60
Figure 4.7	Sample 1, Layers . . . . .	60
Figure 4.8	Sample 1, Layers, Seam Zone . . . . .	61
Figure 4.9	Sample 2, Initial Part . . . . .	62
Figure 4.10	Sample 2, Final Product . . . . .	62
Figure 4.11	Sample 2, Final Product . . . . .	63
Figure 4.12	Sample 2, Layers, Inclination Change Zone . . . . .	63
Figure 4.13	Sample 2, Layers, Inclination Change Zone, Side View for Parallel Lines . . . . .	64
Figure 4.14	Sample 2, Layers, Retraction Effect . . . . .	64
Figure 4.15	Sample 2, Layers, Retraction Effect . . . . .	65

Figure 4.16	Sample 3, Grey Part . . . . .	65
Figure 4.17	Sample 3, Red Part . . . . .	66
Figure 4.18	Sample 3, Final Product . . . . .	66
Figure 4.19	Sample 3, Layers, Black & Red Zones . . . . .	67
Figure 4.20	Sample 3, Layers, Red & Grey Zones . . . . .	67



## LIST OF ABBREVIATIONS

2D	2 Dimensional
3D	3 Dimensional
AM	Additive Manufacturing
Brep	Boundary Representation
CAD	Computer Aided Design
CAM	Computer Aided Manufacturing
DfAM	Design for Additive Manufacturing
DLP	Digital Light Processing
FFF	Fused Filament Fabrication
ILP	Inclined Layer Printing

# CHAPTER 1

## INTRODUCTION

### 1.1 Motivation and Problem Definition

With the expiration of the patent on Fused Filament Fabrication (FFF), there have been numerous research and developments in the technology. By time, Additive Manufacturing (AM) got more affordable and reached wider popularity. There have been many implementations and improvements considering the production processes, such as materials, topology, process optimization, efficiency and others. In this study, two main issues are challenged.

The first one is the implementation of FFF process for mass production. Since the earlier years of the technology, there has been a fixed printing bed where the material has been extruded on during the process. This limits the printing area and the maximum height the nozzle can reach. This is the main limitation against mass production and larger products.

The second challenge is probably the most common topic, optimization of support structures. Support structures are waste of material. Once support structures are built over the artifact, they need to be further processed, which increases the overall fabrication time. Numerous studies were conducted to reduce or remove the need for support structures in FFF processes via various approaches.

In this study, a method is proposed to overcome these challenges, an adaptive slicing algorithm for an inclined FFF 3D printer. The algorithm takes the input geometry, slices adaptively and generates the printing data, to be processed on the inclined 3D printer.

## 1.2 Proposed Methods and Models

The proposed methods and models are divided into two; the algorithm and the machine. The adaptive slicing algorithm simply simulates the inclined 3D printing process. Depending on the support structure data, it proposes an optimized orientation for the geometry. Finally, it generates 3D printing data, similar to the G-Code in traditional manufacturing for the inclined FFF 3D printer.

The inclined FFF 3D printer is where the manufacturing is completed. Similarly, but more complicated compared to the conventional FFF machines, the extruder moves on an inclined plane with respect to the horizontal axis, and instead of extruding onto a classical print bed, a conveyor belt system is included in the assembly.

## 1.3 Contributions and Novelties

The adaptive slicing algorithm gets the input geometry. After the intermediate processes, it provides manufacturing data for the inclined FFF 3D printer. It provides the followings.

- **Inclined Slicing:** Different from the classical approach, the algorithm is designed for inclined 3D printing operations. The slicing layers are not perpendicular to the vertical axis. They are adaptively adjusted depending on the support requirements of the input geometry. After geometric operations, it presents manufacturing data as output.
- **Support Minimization:** The algorithm includes an orientation optimization for the minimum support requirement. It computes the input geometry in different orientations, and by combining it with the adaptive slicing, it offers the least amount of support structures for manufacturing.
- **Infill Geometry:** Similar to the other AM CAM software, the algorithm computes shells and infill data depending on the inputs provided by the users. However, since the manufacturing method is different, it operates for adaptive inclined FFF 3D Printers. In the end, it returns manufacturing data in a form

similar to G-Codes.

In addition, the adaptive inclined FFF 3D printer has a conveyor belt system, which removes the volume limitations of a classical FFF 3D printer. By this way, infinite 3D printing opportunity is enabled as well as the capability of mass manufacturing.

The studies up to now on inclined FFF 3D printers just adjust the slicing plane at fixed angles. Increasing the flexibility on the orientation of the slicing plane and controlling it during the process give the adaptive opportunity, which would further decrease the amount of support structures in the process.

#### **1.4 The Outline of the Thesis**

This thesis is based on a novel idea, adaptive inclined FFF process. It covers basic background regarding related technologies, starting with AM, and narrowing down to FFF, support generation, recent methods for least support generation, inclined 3D printing and mass production with AM throughout Chapter 2. This background chapter does not cover these topics in detail, but concise information is provided to enlighten the reader about the topic and recent studies.

Following the background, in Chapter 3, the thesis briefly describes the adaptive inclined slicing algorithm. The strategy is described by using a sample Mesh & Boundary Representation (Brep), the Stanford Bunny. The steps are given for a fixed orientation, and described in detail. Afterwards, the optimization is explained throughout the different orientations. For a better understanding, flowcharts and pseudocodes are also provided.

Afterwards, manufacturing is explained as well as the required and implemented hardware in Chapter 4. The test prints are given as samples. Finally, in the conclusion part, Chapter 5, the conclusions of the study are provided and the pinpoints are emphasized.



## CHAPTER 2

### BACKGROUND

#### 2.1 Introduction

As mentioned in Chapter 1, brief background information is provided in this chapter. The topics continuously narrow down, starting with AM and continues through FFF, Support Generation, Design for Additive Manufacturing (DfAM) and finally Continuous 3D Printing & Mass Production with AM. Recent studies on these topics are elaborated before giving detailed information about the main algorithm in Chapter 3.

#### 2.2 Additive Manufacturing

It has been more than 30 years since the term *Additive Manufacturing* come up. It was a revolution in manufacturing and since then, it has constantly been evolving. By time, many new methods and many different approaches have arisen to improve this technology.

In traditional manufacturing, which is also referred as subtractive manufacturing, desired parts of a block material are removed by cutting tools. On contrary, in AM, by adding layers successively in several methods, a new product is formed. Both methods offer different opportunities. Depending on the desired product specifications and expectations, the manufacturing approach can be chosen. There are also many studies to ease the decision by considering different aspects [1–4].

In additive manufacturing, .stl files are used to define the geometry. CAD software slice the geometry into the desired layer thicknesses, and combine these slices to

form the artifact. The output .stl file is sent to the Computer Aided Manufacturing (CAM) software. The software prepares the printing process, creates shells, support structures and infill patterns depending on the parameters set by the users. In the end, it provides a manufacturing data, similar to G-Codes in traditional manufacturing processes. Depending on the AM method, the process follows up.

### 2.3 Fused Filament Fabrication

The most common AM method is Fused Filament Fabrication (FFF). The beginning of Rapid Prototyping (or with a popular name, 3D Printing) is Fused Filament Fabrication, which was started and commercialized by Stratasys in 1992. The original name of the patent filed by the company was "Apparatus and method for creating three-dimensional objects" [5].

In FFF technology, there is a heating chamber, which is also referred as the print head or extrusion head, where the polymer supplied to the system in the form of filament by a spool liquefies. By this way, the liquid (or semi-solid) polymer is extruded through the nozzle continuously onto a platform, named printer bed, and it is completely solidified there. Layer by layer, the process continues, and in the end, a final product is obtained. A simple illustration is given in Figure 2.1.

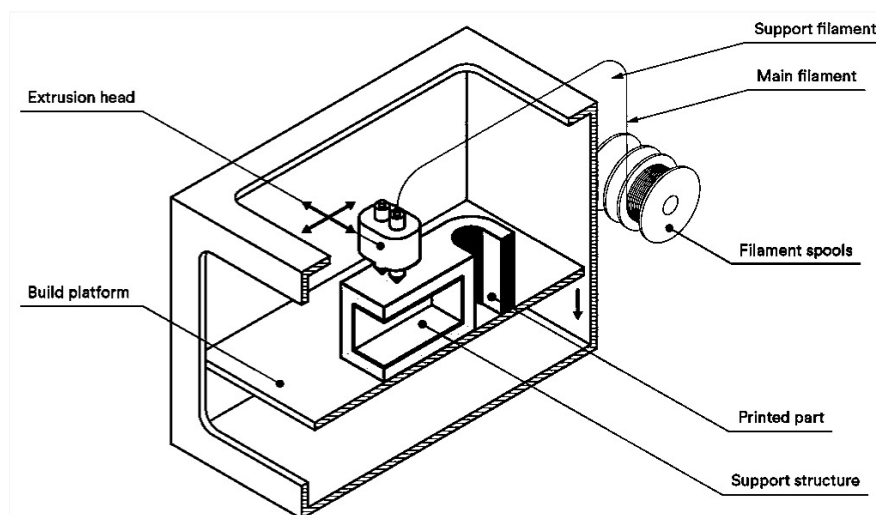


Figure 2.1: A Standard Fused Filament Fabrication Setup [6]

As the technology gets more and more popular and widespread, there have been many research in the area focused on materials, support structures, mass production, design for additive manufacturing, control, speed, surface quality and many other topics.

### 2.3.1 Parameters in Fused Filament Fabrication

In order to understand the volume calculations in Chapter 3, where the algorithm is presented, brief information on 3D printing parameters is given in this chapter. Only the items affecting the volume and process of adaptive slicing algorithm are described.

- **Nozzle Diameter:** The diameter of the material extruded through the nozzle. It directly affects the quality of the product on the XY-plane. Lower diameter results in better precision, better quality, but lower printing speed.
- **Infill Density:** The ratio of filled material to the overall volume of the product. It can vary from 0 (hollow part) to 100 (solid part). Higher infill density would result in higher strength, whereas it drastically affects the duration of the printing process.
- **Layer Thickness:** The thickness of successive layers in the printing process. Similar to the nozzle diameter, it is a condition between quality and printing speed. Lower layer thicknesses increase the overall quality of the product between successive layers in the Z-Axis.
- **Shell Thickness & Number of Shells:** Shell can be simply defined as the outermost profile of the product. Since the quality of this part of the product is the major concern, it can be editable separately from the infill details. The number of shells is how many offset profiles are set and the thickness is the difference between these profiles, both are trade-offs between quality and printing speed.

These parameters and more features such as temperature and infill pattern can be adjusted by the CAM software. The software would give the required manufacturing process data, which can be read and processed by the 3D printer itself.

## 2.4 Generation of Support Structures

The additional structures extruded which are not parts of the product in an FFF process are referred as support structures. Support structures are required to hold the upcoming layers in the overhanging or bridging situations. However, they are simply waste of materials, which requires post-processing after the main manufacturing operation. In Figure 2.2, three letter samples are provided. Considering the Y letter, the overhanging zones do not have a higher angle than the critical angle. However, for the H and T letters, the bridging and overhanging zones require support structures since these zones are directly perpendicular to the printing axis.



Figure 2.2: Sample Cases for Overhanging and Bridging Support Requirements [7].

Since the start of the technology, support structures have been the main research area in the process. There are studies to recycle the waste support materials as well as easing the post-processing. These studies include recycling processes and life-cycle analysis of the FFF filaments [8], separation of support material from the product without damaging by using solvable support materials and many others.

Directly eliminating and reducing the need for support structures are the most efficient options, but they are also the most challenging ones. There are many approaches to handle the overhanging and bridging volumes. In the upcoming subtopics, some of the approaches and studies to eliminate or reduce the support structures are given.

### 2.4.1 Object Partitioning

Object partitioning is the strategy where the product is subdivided into smaller parts. These sub-parts are found by an algorithm such that none of the sub-parts would require support material. They are manufactured separately, and afterwards they are merged into a major assembly, which is the main product. Karasik et al. [9] published an algorithm to divide any geometry depending on the critical angle of the process. As illustrated in Figure 2.3, the products are divided into sub-parts, 3D printed separately in different colours and assembled afterwards.

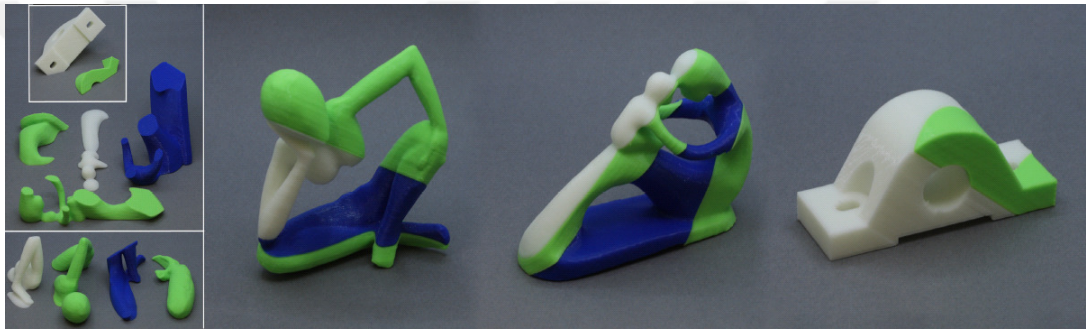


Figure 2.3: Object partitioning sample, the sub-parts assembled to eliminate the support structure requirement [9].

For combining, there are again different approaches. Depending on the need of the product, appropriate glues can be used. Depending on the product's working conditions, a glue is chosen and used to simply stick minor parts. For better adhesion, different geometries and materials are combined with different kinds of glues [10]. There are also many studies for medical operations and biologically harmless glues [11]. Another option is using interlocking, where these smaller gaps contain an inner cavity, and an additional part is manufactured, simply in order to lock and combine these cavities. Wang et al. [12] proposed an approach where the parts have bulges as well as cavities. Similar to LEGO Bricks, the parts fit into each other depending on the final geometry.

## 2.4.2 Inclination

Inclination is another alternative approach to eliminate or reduce the support need. In this strategy, the extrusion operation in 3D printing process is inclined by an angle, depending on the geometrical needs. Given in Figure 2.4, the overhanging and bridging parts of a geometry can be manufactured without a need for support structures in some cases. This is possible in two ways.

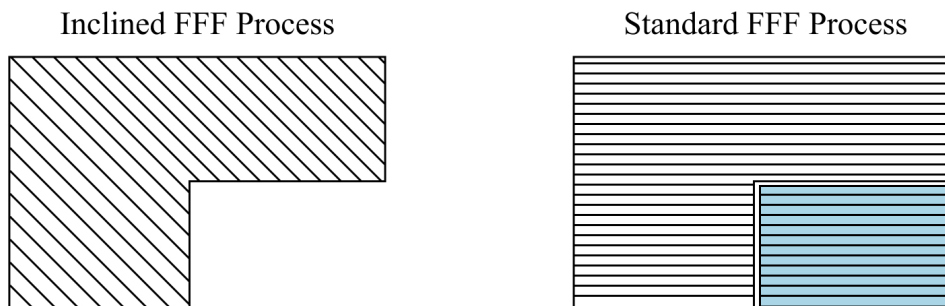


Figure 2.4: Comparison of inclined and conventional FFF processes.

Firstly, the nozzle can be inclined by an angle. In classical FFF approach, the nozzle is directly perpendicular to the print bed, which is commonly referred as Z-axis in the 3D printing space. Extrusion is also maintained in the Z-axis, and considering the whole process, it stores less space, and the operation can be controlled easily. However, if these advantages are dismissed and the nozzle is inclined by an angle, support requirement of certain geometries can be prevented, Figure 2.4. This approach requires a larger space, but this disadvantage can be prevented and even becomes an advantage if a conveyor system is used, similar to the technology used by Blackbelt 3D. Use of conveyor belt and improving the process for mass production are further investigated in the upcoming subsections.

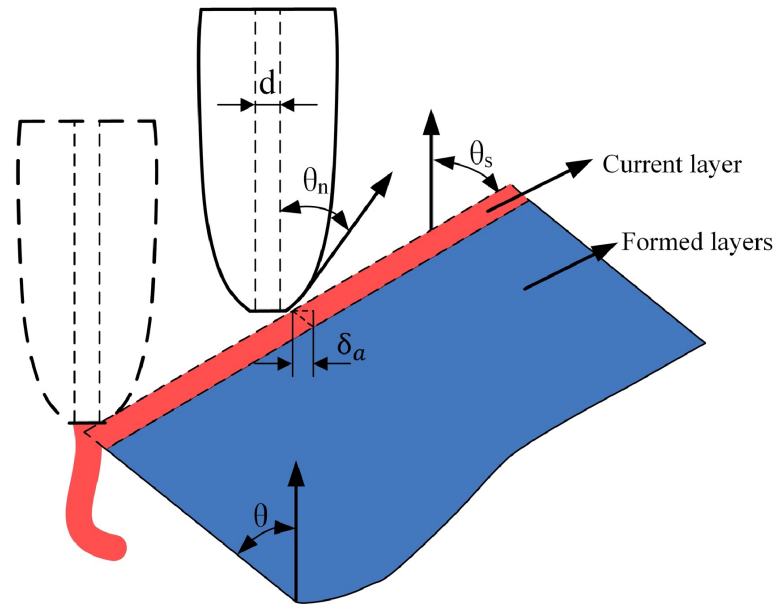


Figure 2.5: Inclined layer printing process [13]

Another way to incline the extrusion operation is inclining the nozzle path. In this approach, the nozzle is not directly rotated. It is kept perpendicular to the printing bed. However, the nozzle may move with an angle corresponding to the z-axis to prevent the need for support structures in certain geometries [13]. The implementation of the strategy is further given as 2.5. Depending on the projection of the geometry, the product is partitioned. The support needs and the required printing/layer angle in the respective sub-part are generated, and the operation moves on with respect to these factors. By this method, the space requirement in the earlier approach is eliminated since the nozzle is perpendicular to the print bed. The control of the process is relatively more complicated, and the conveyor approach is less likely to be implementable.

### 2.4.3 Shape & Support Modification

Another way to reduce the amount of materials used in support structures is modifying the shape of the part. In this method, the desired output geometry is modified for less support requirement and the overall product quality is improved by several different approaches. The CAM software, the algorithm transforms the geometry into a shape

that requires less support structures as well as avoiding the staircase effects in the rounded parts of the input geometry [14]. After computation, it gives feedback to the user, and the user may prefer to change its initial design.

As well as adjusting the main product, support structures can be adjusted to the minimize waste. In classical approach, any support structure required to hold the overhanging or bridging volumes are simply shadowed regions of the product, with reduced infill ratio, so that it can be separated easily.



Figure 2.6: Support volume reduction by modification [15]

However, this waste can be minimized by using topology and material analysis. Instead of piling up layers and layers of support material, placing a few respective structures to hold the critical regions can solve the problem. Hu et al. [15] proposed a study where the support structures are slimmed in the chosen sub volumes in DLP as given in Figure 2.6. In these methods, the lack of chosen support volumes does not damage the operation. Kuo et al. [16] proposed an approach where the easy removal requirement and the amount of support waste is considered as a trade-off .

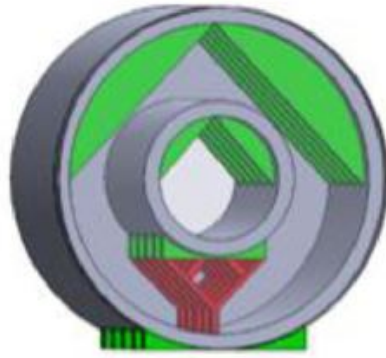


Figure 2.7: Support volume reducing by modification [17]

Jiang et al. [17] proposed a study for the infill volume of the product. By generating parametric infill and support zones with respect to the input geometry, a strong hollow product can be printed, given in Figure 2.7.

#### **2.4.4 Multi-Axis Additive Manufacturing**

Being a revolutionary approach in traditional machining, multi-axis methods are also applied on AM methods. Similar to its traditional versions, adding one or more extra operational axis on the 3D printing offers a great freedom to the process.

In Figure 2.8, a rotating printing bed study is given. Dai et al. [18] set a moving printing bed to offer an additional degree of freedom to the operation. After configuring the CAM software, the product is sliced and manufacturing data is obtained with an additional axis in the system.

Making adjustments on the nozzle plane is another option. De Becker et al. [19] placed three extruder nozzles onto a robotic arm, shown as Figure 2.9. By this way, the process gained more degrees of freedom and more complex parts could be printed without support structures.

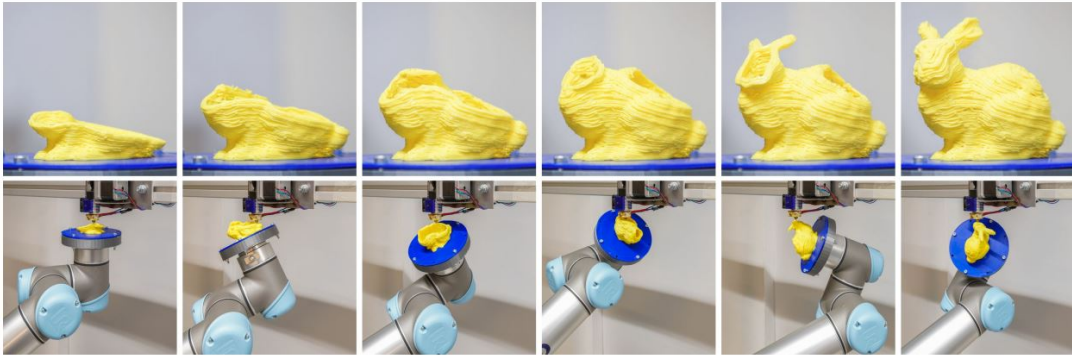


Figure 2.8: Multi-axis AM with a moving printer bed [18]

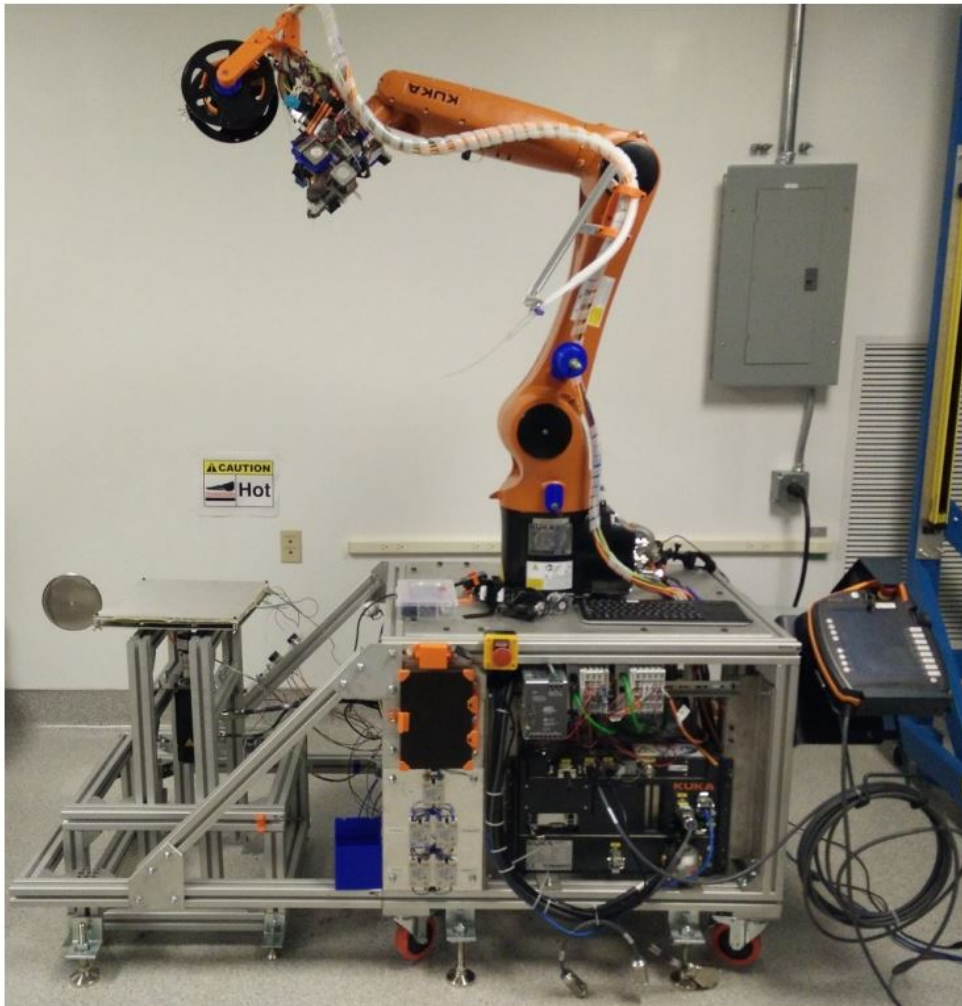


Figure 2.9: Multi-Axis 3D printer with multiple nozzles [19]

## **2.5 Design for Additive Manufacturing**

Design for Manufacturing refers to the idea, where the designer considers the traditional machining while designing the parts. This includes manufacturability, low cost and time considerations, easier processing and any other parameters that affect the production efficiency.

Since the whole manufacturing process in traditional machining and additive manufacturing are different, the design considerations and ideas differ as well. In traditional machining, a block is the primary material, and by simply subtracting material from the product, by using cutters and drillers which further become waste material. On the contrary, in the FFF process, there is no primary block, the material is molten and extruded through the nozzle.

As the manufacturing process is different, the design process has to be modified accordingly, which brought up a new discipline, Design for Additive Manufacturing (DfAM). Executing proper DfAM techniques can save time and costs as well as strengthening up the product, optimizing the process and using 3D Printers efficiently. The DfAM process is widely studied from opportunities to limitations to optimize the whole process. [20, 21]. Sample workflows and frameworks for different processes are inspected with possible future improvements.

There are benefits and drawbacks of using AM methods. Before taking any critical actions for the manufacturing process, the DfAM process must be studied carefully and effectively to reduce waste in the process [22].

## **2.6 Continuous 3D Printing & Mass Production with Additive Manufacturing**

In the FFF process, the printing volume has been one of the common research topics. The volume is limited by the area of the printing bed on the XY Plane, and the maximum possible nozzle height through the Z-axis. In the Figure 2.10, the maximum volume capabilities of different products of 3D Printer manufacturers are given as example [23].

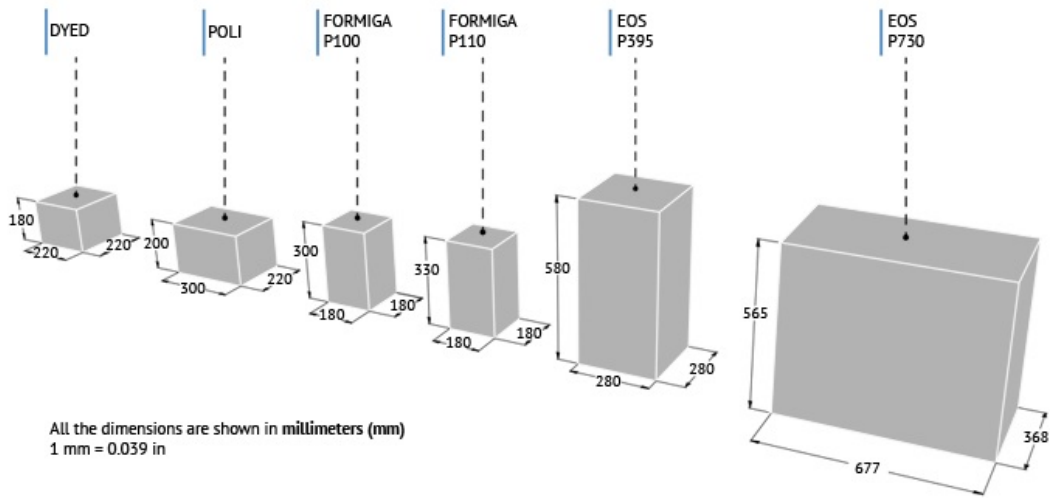


Figure 2.10: Volume limitations of various 3D printers. [23]

Since pre-process and post-process take large amount of times, larger building volumes offer more efficient manufacturing operations. It has also been a major concern to use this volume as efficiently as possible. Jiang et al. [24] prepared an algorithm where the users upload their different batch geometries to the CAM software, and afterwards the algorithm places them such that the least amount of material is used.

Prior to the recent studies, the only enlargements have been expanding the lengths of these limitations, using larger printing beds and higher nozzle height capabilities. Velez et al. [25] implemented the FFF nozzle system on a climbing robot to increase the height of the printing volume, as provided in Figure 2.11. Zhang et al. [26] used mobile robots, which are programmed to work collaboratively on larger surfaces to increase the XY-Plane limitation.

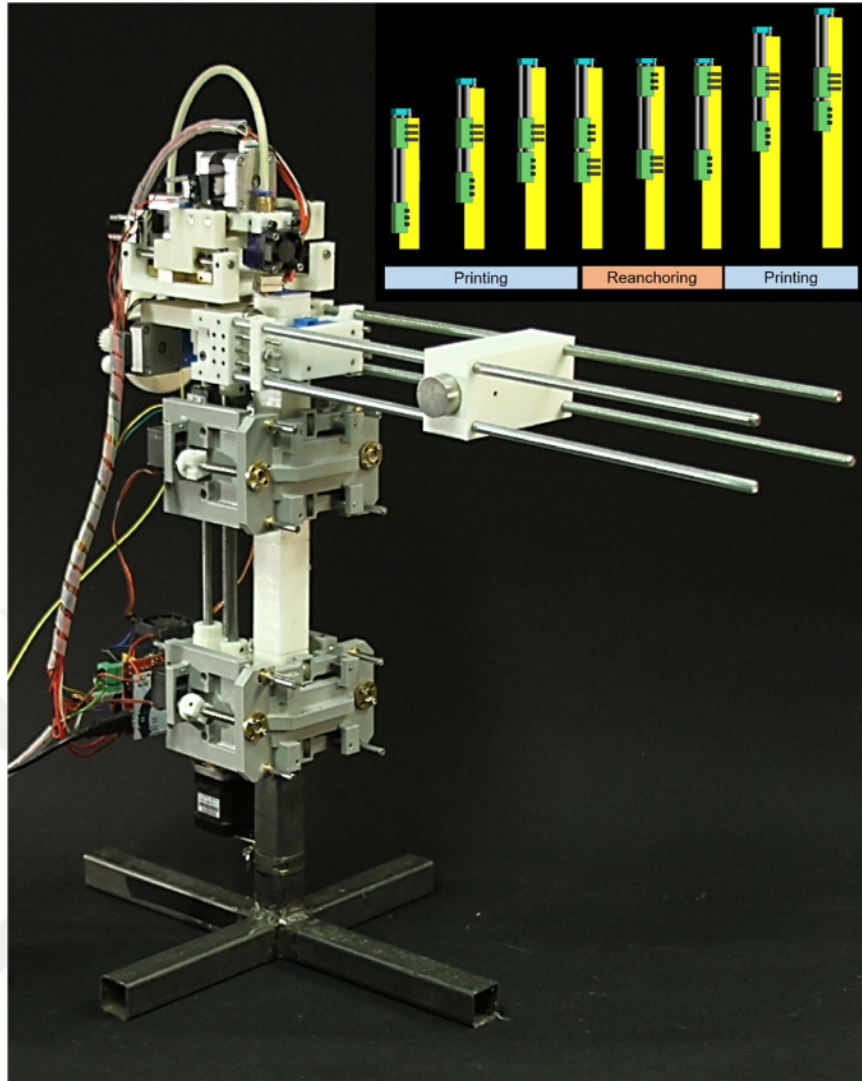


Figure 2.11: Koala 3D, a continuous climbing 3D printer [25]

Another important issue has been the implementation of 3D printing for mass production. In a simple FFF machine, the printing bed is fixed, the printing duration is relatively long and there are also preparation and post-processing periods, which even increase the duration. Although it is acceptable and applicable to agile production systems, this negative effect has been a major concern in lean mass production systems.

Considering these, a new approach is applied to the process, which is widely used in mass manufacturing, conveyor systems. By the application of two basic principles, tilting the nozzle and replacing the bed with a belt, a continuous method can be

formed. Using a belt as a bed means the user can 3D print continuously, whether to produce many regular-sized models or one and extremely long parts.

Blackbelt 3DpPrinter, given in Figure 2.12, is the pioneer of belt FFF 3D printing [27]. It started as a Kickstarter campaign in 2017 by Blackbelt 3D, a Dutch company whose stated goal is to encourage innovation in 3D printing. It has a large XY-Plane build area with an optional configuration to get the printer in a table setup. To ease the adhesion, the bed temperature can be increased up to 140 °C.



Figure 2.12: Inclined 3D printer with a conveyor belt, BlackBelt 3D [27]

Creality, also produced an infinite 3D printer, a more budget version [28]. Similar to the Blackbelt, the company inclined the XY-Plane by a fixed 45°. As given in Figure 2.13, it offers less space, less specifications, but cheaper access to the conveyor belt inclined 3D printers.

Although there are some other lab-scale conveyor belt 3D printing systems, there are not many differences in the main design idea [29, 30]. In this study, it is aimed to increase the flexibility of the system, changing the inclination angle during the process to reduce the amount of support structures required in the system.

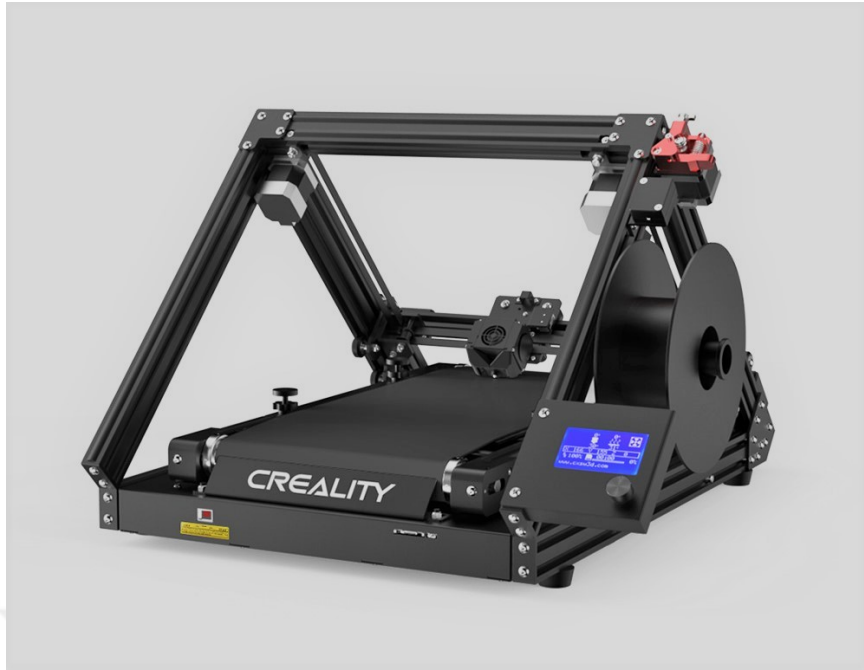


Figure 2.13: Inclined 3D printer with a conveyor belt, Creality CR-30 [28].



## CHAPTER 3

### ADAPTIVE INCLINED SLICING ALGORITHM

#### 3.1 Introduction

The algorithm for the adaptive inclined slicing is presented in this chapter. It is developed in Grasshopper3D, which is an analytical modeling tool for the Rhinoceros3D Software. As well as having its own visual scripting tools, it also has syntax for Python and C# programming languages.

This chapter starts with brief information on the Tree-Branch structures used in Grasshopper3D to prevent data overlaps. Then, a flowchart is provided to guide the reader throughout the algorithm. The required inputs are given and then the steps of the algorithm are explained with a sample geometry, the Stanford Bunny. The steps are grouped as main and sub-topics to ease the following of the process. The main steps of the algorithm are as follows.

- Slicing
- Support Derivation & Optimization
- Shell & Infill Patterns
- Manufacturing Data

## 3.2 Tree Structure & Flowchart

### 3.2.1 Tree Structure

In order not to mismatch any data and prevent data overlaps in the project, Grasshopper3D software uses a Tree-Branch system to store the data. The tree starts with a root. Whenever additional data in the lower level is derived, it is transformed into the branches, which are connected to this root. Similarly, any additional applications on previous data would transform into further tree branches. Each concurrent data is stored in the respective levels on the tree branch levels. This system avoids conflicts and misinterpretations in the data levels and blocks problems.

In the adaptive slicing algorithm, the base geometry can be considered as the root. An example tree and further levels are given in Figure 3.1.

- Level 0: Base Geometry
- Level 1: Orientations of the Geometry
- Level 2: Sub Geometries, Divided by Inclined Layers
- Level 3: Additional data, such as projections, infill patterns and other computations

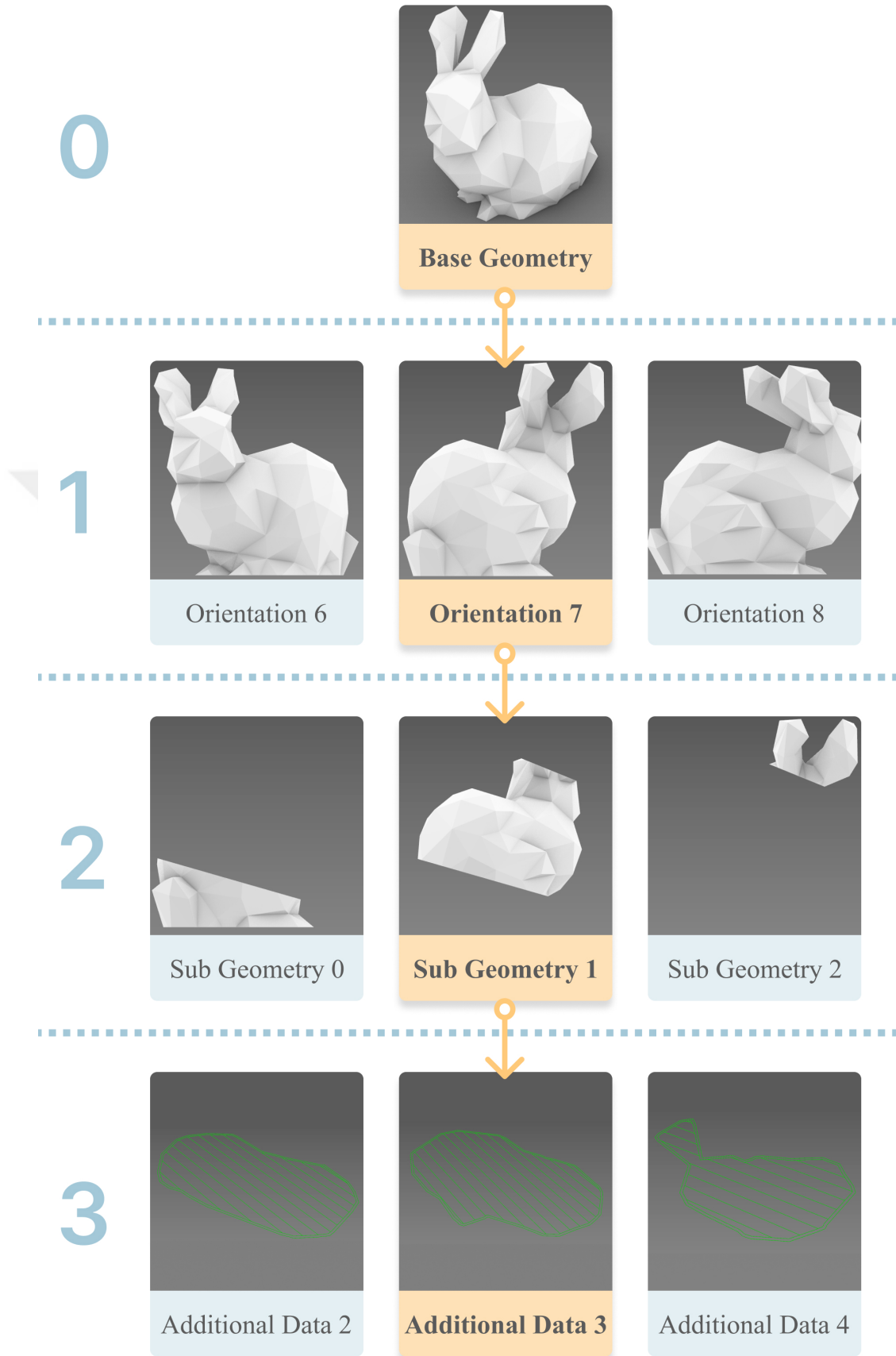


Figure 3.1: Example tree path for {0;7;1;3}

### 3.2.2 Flowchart

In order to ease readability of the process, a flowchart is prepared, Figure 3.2. It can be a guide throughout this chapter.

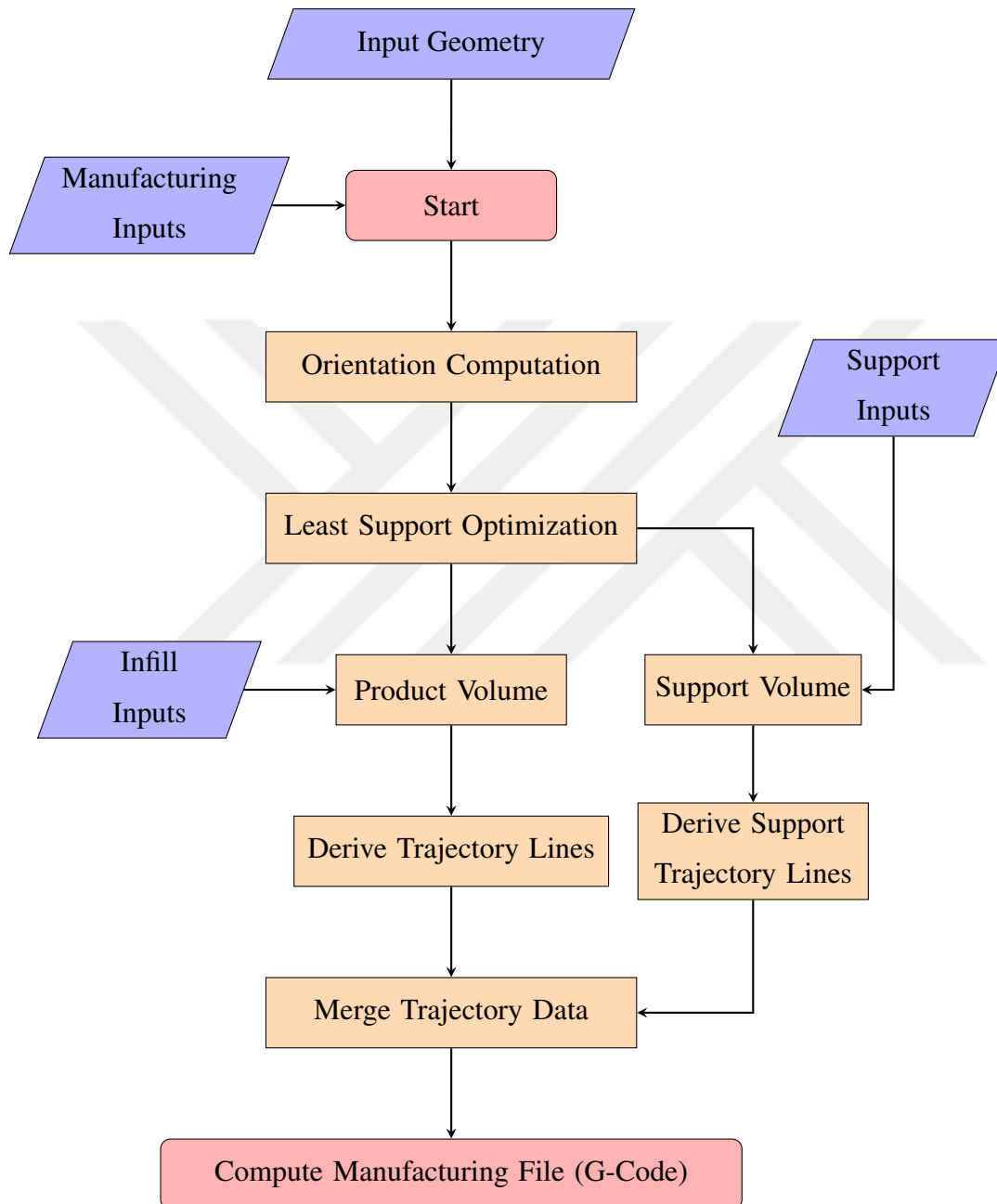


Figure 3.2: Process flowchart

In addition to the previous flowchart, another one defining the orientation computation process is provided in Figure 3.3.

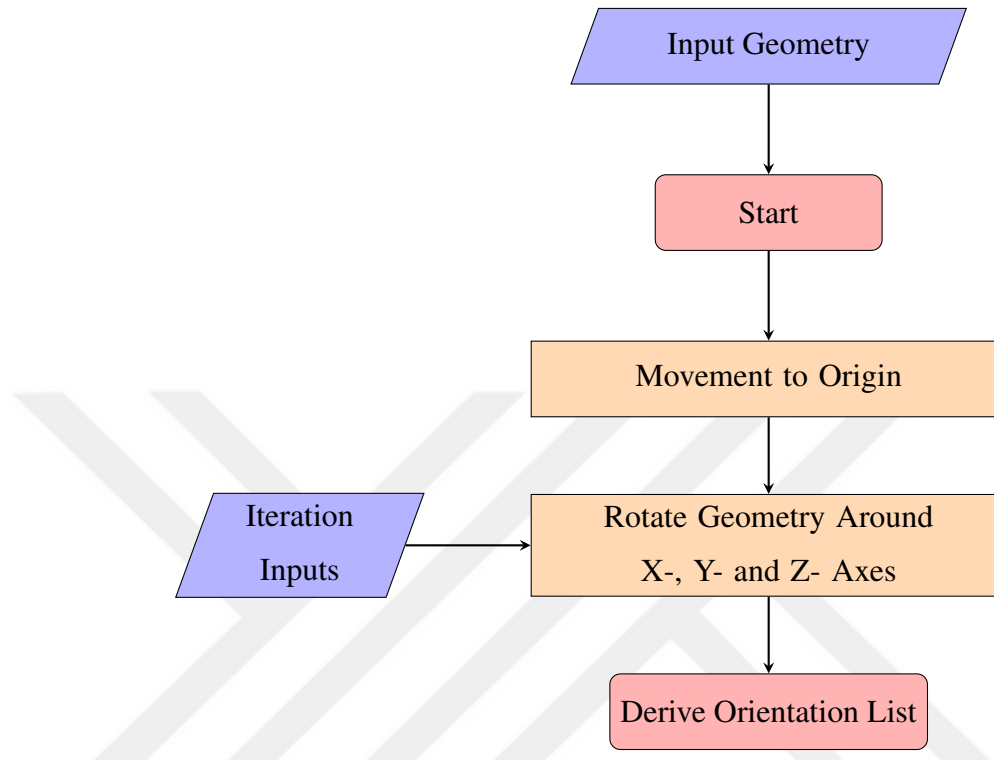


Figure 3.3: Flowchart of the orientation computation

Furthermore, a flowchart to describe the least support optimization process is given in Figure 3.4. That can be considered as the most important part of the main algorithm for adaptive inclined slicing approach.

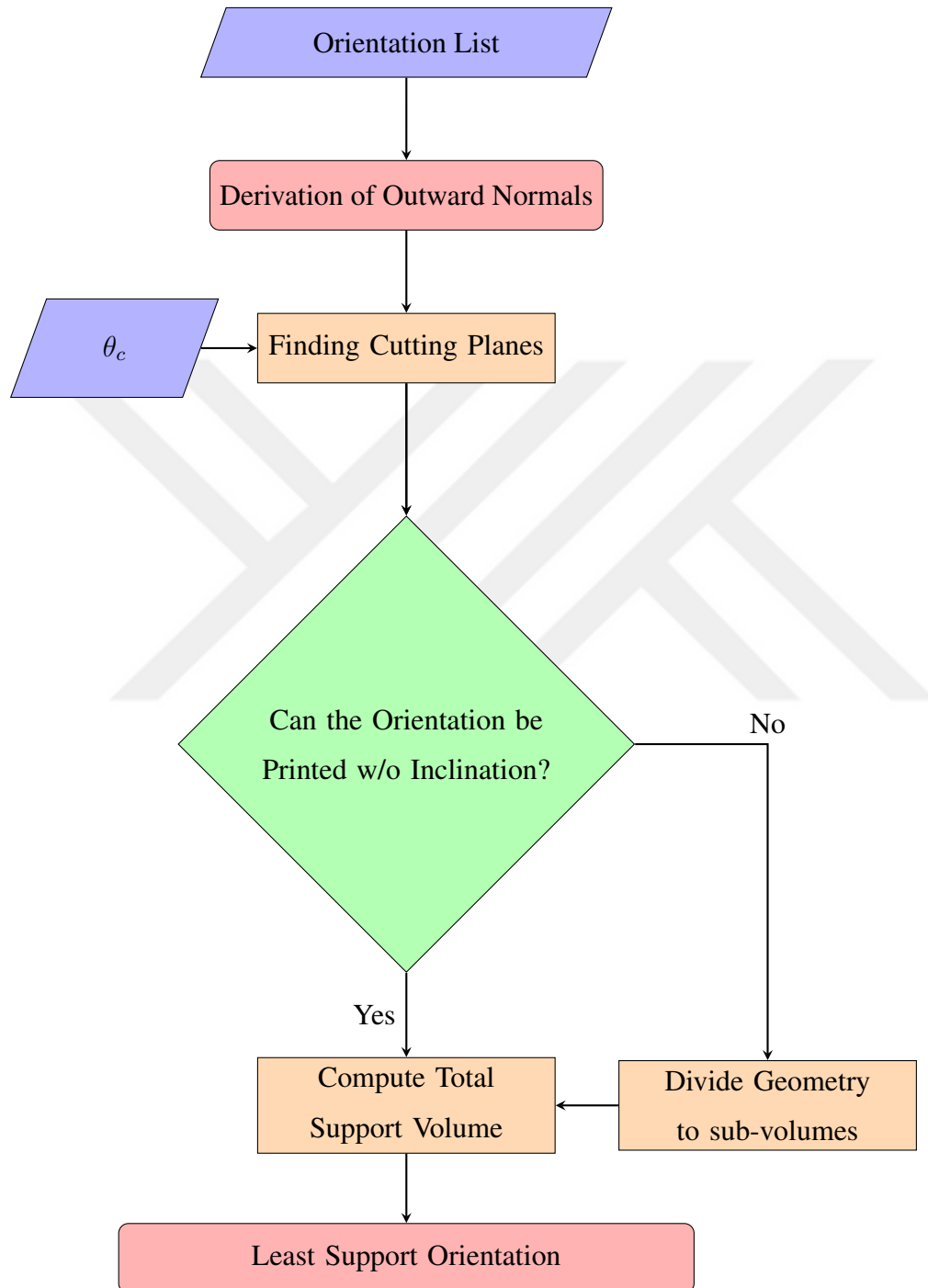


Figure 3.4: Flowchart of the least support optimization

### 3.3 Inputs

The algorithm gets the below inputs, process them and outputs the best orientation and other related manufacturing data.

- **Input Geometry:** This is the geometry of the part to be fabricated. It can be a mesh or a Boundary Representation (Brep) file.
- **Nozzle Diameter:** The diameter of the extruder nozzle is required for slicing and deriving the printing trajectories.
- **Infill Density:** In AM, most of the time, not all of the interior volume is filled to decrease the amount of material utilized and fabrication time. The infill pattern used in the algorithm is a parallel lining. However, with simple adjustments, the pattern may be changed.
- **Support Infill Density:** Similar to the infill ratio, support infill ratio represents the percentage of material in the support volumes. It might be lower than infill ratio.
- **Shell Parameters:** Shells represent the surroundings of the infill, resulting in the outermost profile. They are computed separately to control the outermost surface quality of the profile. The number of shells and shell distance inputs are used to set the quality of the product.
- **Support Requirement Angle:** Although  $45^\circ (\pi/4)$  is commonly accepted as the critical angle where support structures may be needed, in some operations, it may be modified.
- **Layer Thickness:** It is the difference between two consecutive layers. Lower layer thickness would result in better quality and finishing, but it requires more time for fabrication.

In this study, the Stanford Bunny is used as the sample Mesh/Brep, as given in Figure 3.5 and the upcoming figures. The process throughout the algorithm is described with this geometry. The Stanford Bunny is probably the most famous benchmark model in

computer graphics. Being widely used as well in AM, it was assembled from images of a clay bunny [31]. For a faster processing, a reduced mesh quality is employed.

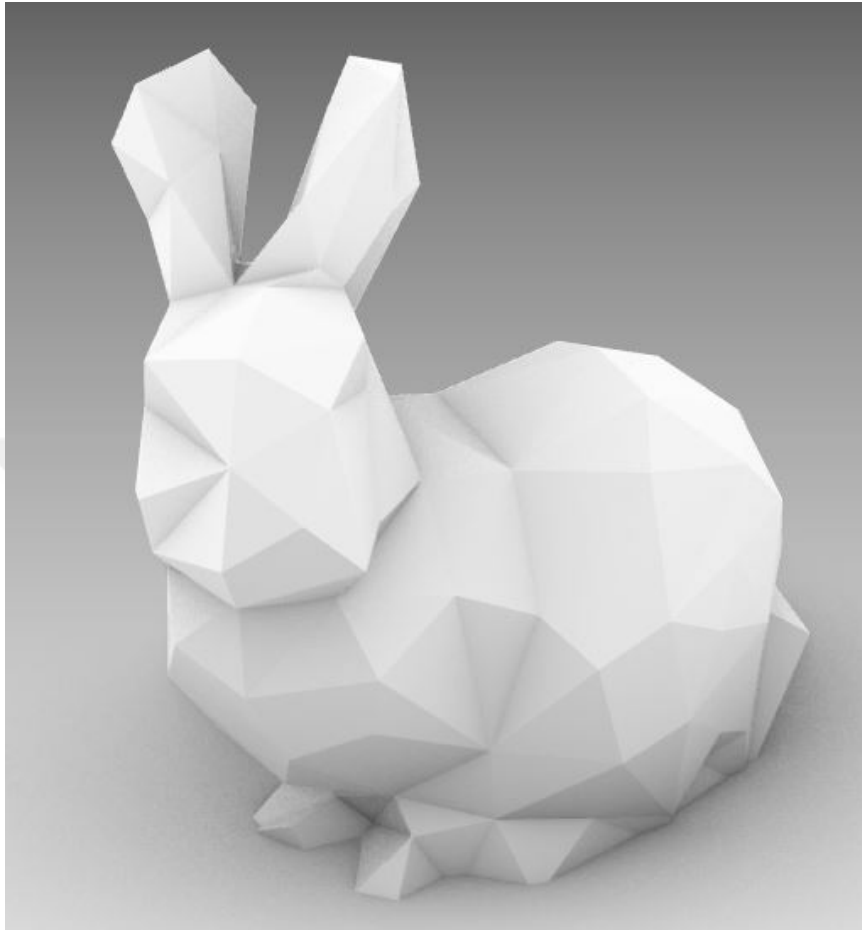


Figure 3.5: The Stanford Bunny, low poly version.

### 3.4 Slicing

In this initial part of the algorithm, the input geometry is duplicated at different orientations and projected onto XZ-Plane for 2D operations. For each orientation, by using the adaptivity script, the printing layers for the minimum support material are derived.

### 3.4.1 Initial Movement & Projection

This subsection starts with a non-mandatory step, the initial movement, which is included in order to set the position of the product. The reason is to set the initial plane on the origin of the space, which is required for the latter stages of the algorithm.



Figure 3.6: The Stanford Bunny, sample orientation

The moved geometry is then rotated around X, Y and Z-Axes, depending on the increments entered in the input part by the user and a list of geometries in different orientations is derived. This list represents the first level of the Tree-Branch System. Each orientation in this list increases the potential to find the optimum geometry with the least support material. On the other hand, the algorithm would require a longer duration, since each orientation has to be computed until the volume calculations. In this example, a single orientation is chosen, given as Figure 3.6, and all the following

steps are processed using this sample.

Afterwards, 2D Projections of the geometry are taken onto the XZ Plane. Here, for each projected orientation, the GhPython Script derives the inclined slicing layers. For this purpose, first of all, the outer profile of the projection is taken and it is split into the line segments. The pin point on the left bottom of the profile is aligned to the origin. With the neighbour points, the initial layer is obtained.

Following this, the normal vectors perpendicular to each segment of the outer profile are derived. Depending on the direction of these normals, the script either may change the printing angle,  $\theta_p$ , or keep it constant.

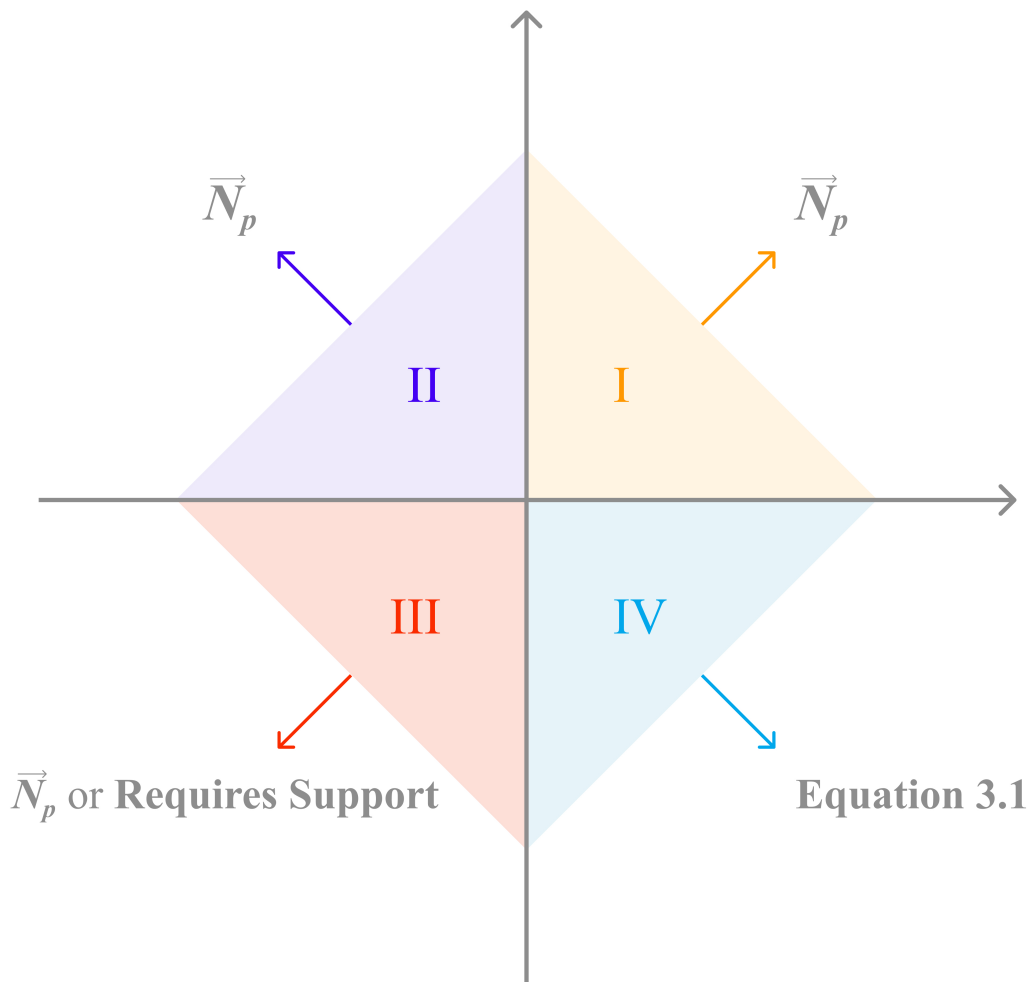


Figure 3.7: Angle sectors and conditions

To illustrate the derivation, a brief example is given in Figure 3.7. The outward normals of the profile are the key to the adaptivity approach. The printing orientation is directed to Sector I. Since upward normals do not require support material, the line segments whose normal vector is directed to the Sectors I and II do not affect the adaptivity. These zones can be printed directly, without a need of inclination angle change (kept as  $\vec{N}_p$ ). Considering the Sector III, the printing orientation is directly opposite. Consequently, if this part cannot be printed by using the current printing angle, it would require support material.

Considering the case where the outward normal is directed to the Sector IV, the script uses the condition given as Equation 3.1. If the angle between the corresponding segment's outward normal and current printing normal is higher than the critical angle,  $\theta_c$ , the angle changes by a step, depending on these vectors' average. By this way, the support requirement at this zone is eliminated. The further segments would continue with the new printing normal.

$$\vec{N}_p = \begin{cases} (\vec{N}_p + \vec{N}_i), & \text{if } \angle(\vec{N}_p, \vec{N}_i) > \theta_c \\ \vec{N}_p, & \text{otherwise.} \end{cases} \quad (3.1)$$

The brief pseudocode of the process is given in Algorithm 3.1. A process example for the Algorithm is also provided in Figure 3.8. For the given orientation, the initial layer is computed as the purple line. The printing normal is perpendicular to this line, which is represented as the green vector. The slicing process continues, with the green lines until a shape change in the outer profile, when a new line segment comes up. At these tip points, if the segment's outward normal is directed to the Sector IV, the conditional statement, given in Equation 3.1 is applied and the printing angle is changed if required.

---

**Algorithm 3.1** Slicing & Layer Derivation
 

---

- 1: **Input:**  $O_i$ : Orientations of Input Geometry
  - 2: **Input:**  $\vec{N}_{p_i}$ : Printing Normal
  - 3: **Input:**  $C_i$ : Cutting Plane List of Orientation  $i$
  - 4: **Output:** Orientation with the Least Support Volume
  - 5: **for** Every Orientation  $O_0, O_1, O_2 \dots O_i$  **do**
  - 6:     Derive the Outer Profile  $P_0, P_1, P_2 \dots P_i$
  - 7:     **for** Every  $P_i$  **do**
  - 8:         Divide  $P_i$  into Line Segments,  $L_{00}, L_{01}, L_{02} \dots L_{10}, L_{11}, L_{12} \dots L_{ij}$
  - 9:         Derive the Outward Normals,  $\vec{N}_{00}, \vec{N}_{01}, \vec{N}_{02} \dots \vec{N}_{10}, \vec{N}_{11}, \vec{N}_{12} \dots \vec{N}_{ij}$
  - 10:         Compute the Initial Layer,  $IL_0, IL_1, IL_2 \dots IL_i$
  - 11:         Printing Normal  $\vec{N}_{p_i} = IL_i$
  - 12:         Append  $\vec{N}_{p_i}$  to  $C_i$
  - 13:         **if** Any  $\angle(\vec{N}_{ij}, \vec{N}_{p_i}) > \theta_c$  **then**
  - 14:              $\vec{N}_{p_i} = \vec{N}_{p_i} + \vec{N}_{ij}$
  - 15:             Append  $\vec{N}_{p_i}$  to  $C_i$
  - 16:         **for** Each Plane in  $C_i$  **do**
  - 17:             Divide  $O_i$  into sub-volumes  $V_{00}, V_{01}, V_{02} \dots V_{10}, V_{11}, V_{12} \dots V_{ij}$
  - 18:             Compute Respective Support Geometries  $S_{00}, S_{01}, S_{02} \dots S_{10}, S_{11}, S_{12} \dots S_{ij}$
  - 19:         Sum Support Volumes  $S_i = \text{sum}(S_{ij})$
  - 20: Find  $\min(S)$  and the respective Orientation
- 

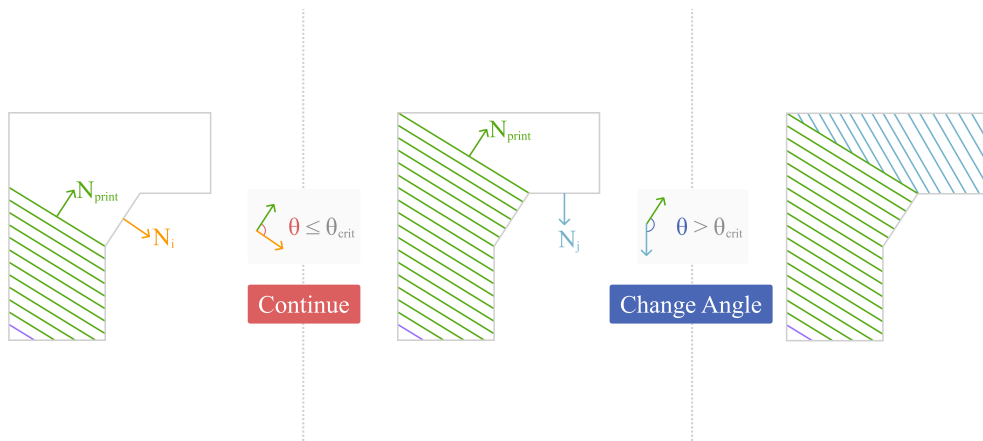


Figure 3.8: Example Process for Slicing

As shown in the Figure 3.8, the slicing process starts with the initial layer up to the first tip point on the right. The angle between the printing normal, green and the corresponding segment's outward normal, orange, is derived, given as red. Since the angle is lower than the critical angle, the printing process continues. Similarly, at the second point, the angle between the printing normal and the corresponding outward normal, blue is derived. The angle between these vectors is higher than the critical angle. Consequently, in order to remove the support requirement, a new printing angle is defined and the process continues until the whole projection is sliced.

The Stanford Bunny sample of the process is given in Figures 3.9 and 3.10. As mentioned earlier, firstly, the outer profile is projected onto the XY-Plane and divided into line segments, shown as green. Afterwards, the initial plane is derived and outward normals are taken for each segment. These normals are shown as blue in the figure. Until the ears of the Bunny, none of the outward normals require additional support structures since all of their angles with the printing normal are lower than the critical angle,  $\theta_c$ . At the lower tip of the ears, a new slicing plane is generated, and the upcoming segments are processed with respect to the new printing normal. In this orientation, two different slicing planes are required (with one inclination change step) which are shown as red.

This process is repeated for all the orientations defined in the input section. As mentioned earlier in Figure 3.1, the orientations are set and stored in a different tree level in order to prevent data overlaps.

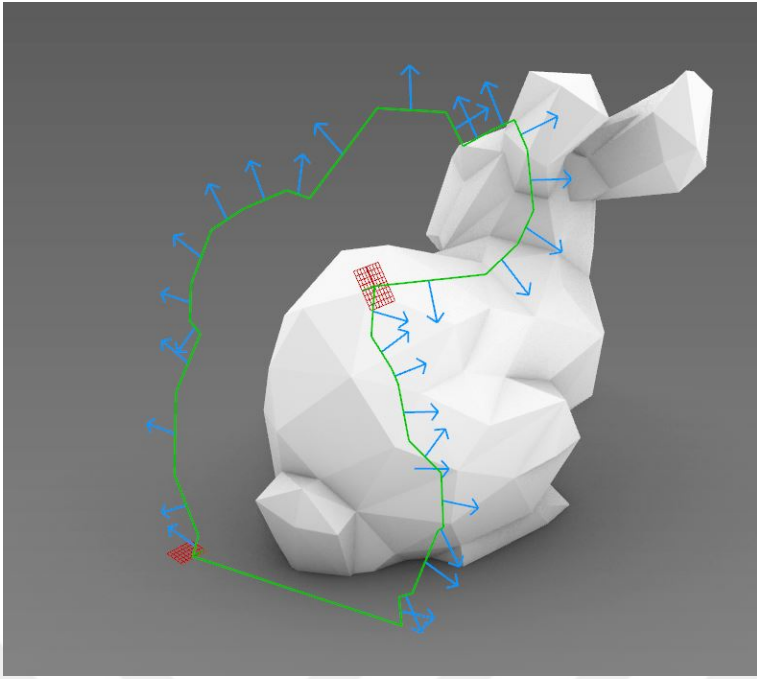


Figure 3.9: Green: Projection | Blue: Outward Normals | Red: Slicing Planes

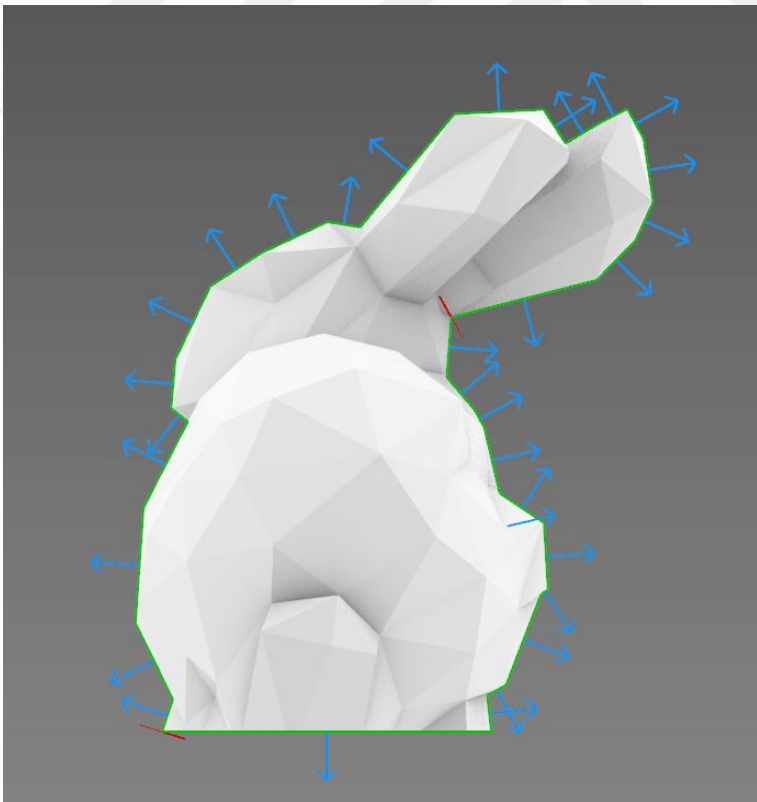


Figure 3.10: Green: Projection | Blue: Outward Normals | Red: Slicing Planes

### 3.5 Support Derivation & Optimization

After the derivation of the printing planes, volumetric operations follow up. The printing planes are used to cut the initial geometry into sub-volumes. After these sub-parts are derived, respective support volumes are computed for all the orientations. In the final subsection, the least support volume optimization is explained.

#### 3.5.1 Object Partition

With the derivation of the slicing planes for all the orientations, the initial geometry is divided to sub-parts, similar to the object partitioning. Each sub-part is additively manufactured with respect to the corresponding plane. Considering the sample orientation, the input geometry had two printing layers as derived in the earlier section, and the Brep is divided accordingly, as given in Figure 3.11.

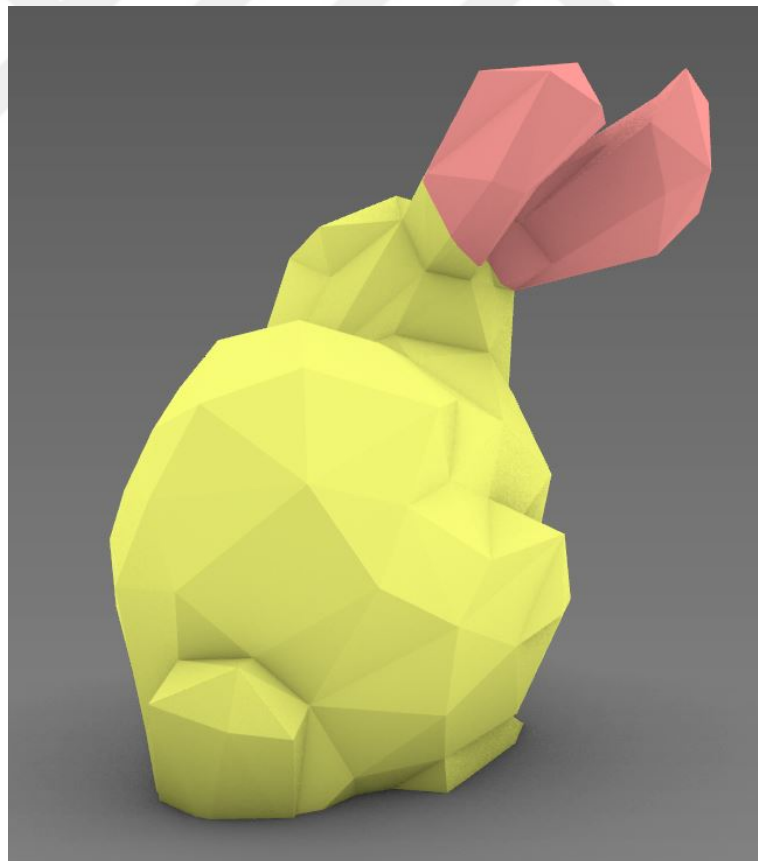


Figure 3.11: The Stanford Bunny, divided

In the sample, any volume between the initial plane and the plane at the lower tip of the ears will be printed with layers parallel to the initial layer. It refers to the yellow volume in the sample, covering from the ground to the ears. Afterwards, the secondary plane comes up, and the rest of the part is printed with respect to the corresponding printing normal and angle, given as the pink volume in the example.

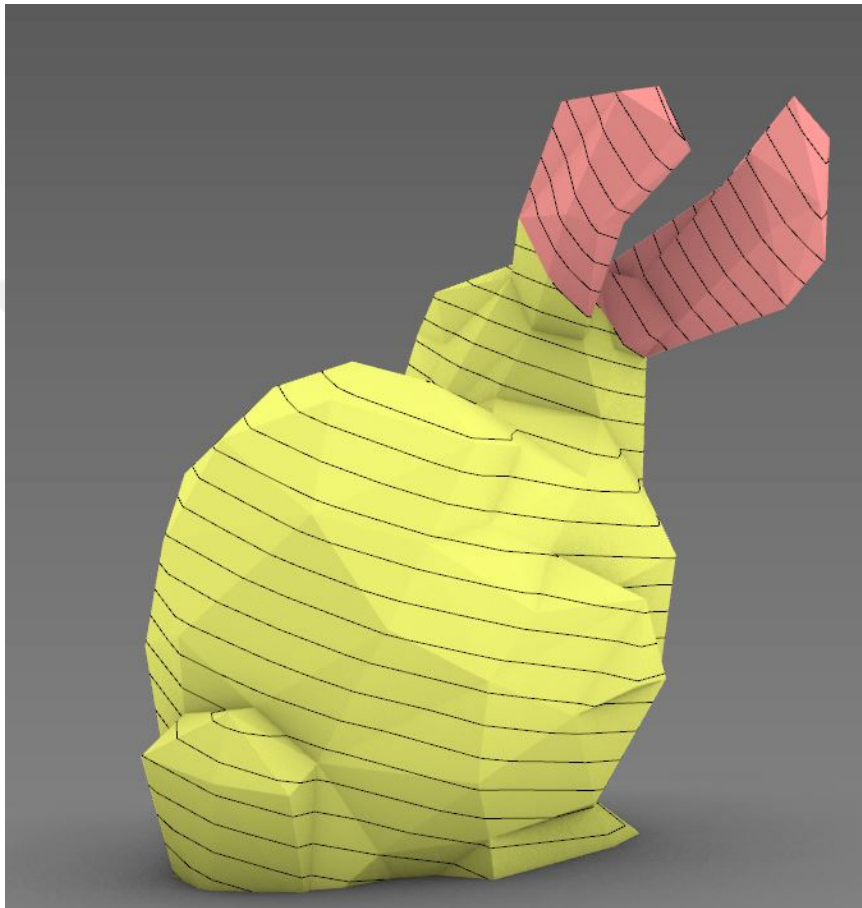


Figure 3.12: The Stanford Bunny, intersected

Now, since the printing planes and their respective volumes are computed, plane arrays can be computed to derive the outer profile of the geometry. The intersecting boundaries are formed with an increment of layer thickness throughout the geometry. The result of this process for the sample is given in Figure 3.12. The layer thickness is exaggerated for simplicity. This process is repeated for all the orientations.

After the boundaries are obtained, each boundary is extruded by a factor equal to the layer thickness. The collection of these sub-volumes represents the outline of the product, given in Figure 3.13. Inside it, the user can choose the desired infill density, which is computed in the upcoming stages.

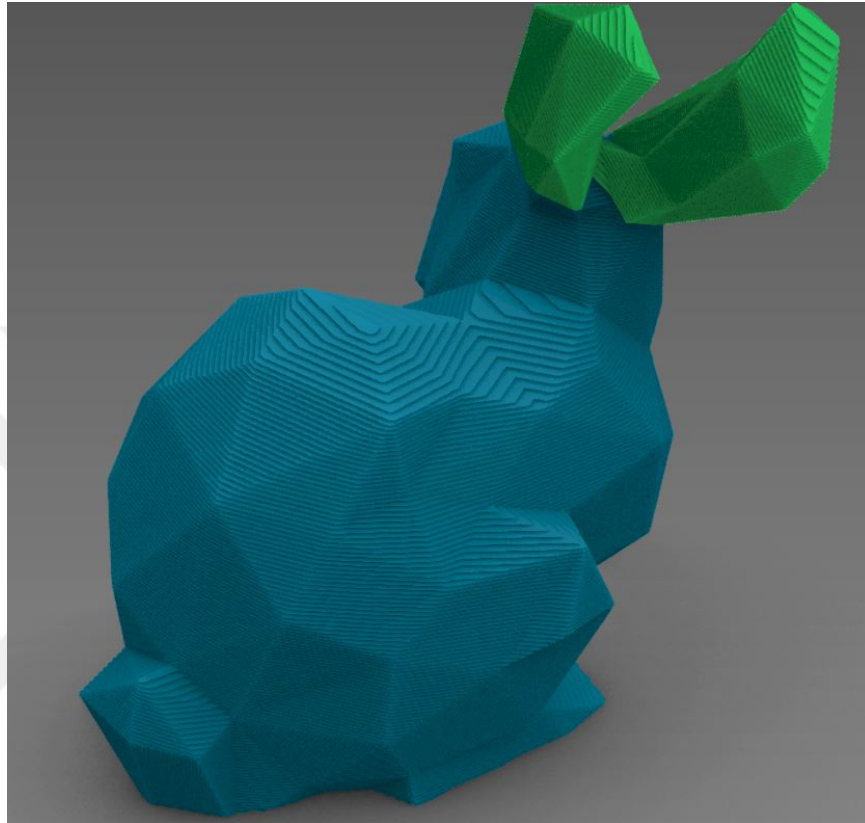


Figure 3.13: Stanford Bunny, Divided, Extruded

### 3.5.2 Support Structures

In this step, the process continues by deriving the support structures on the corresponding orientations, if required so. The volumes are projected and connected to the lower planes, constructing support material where required. An example of the sample case is given in Figure 3.14

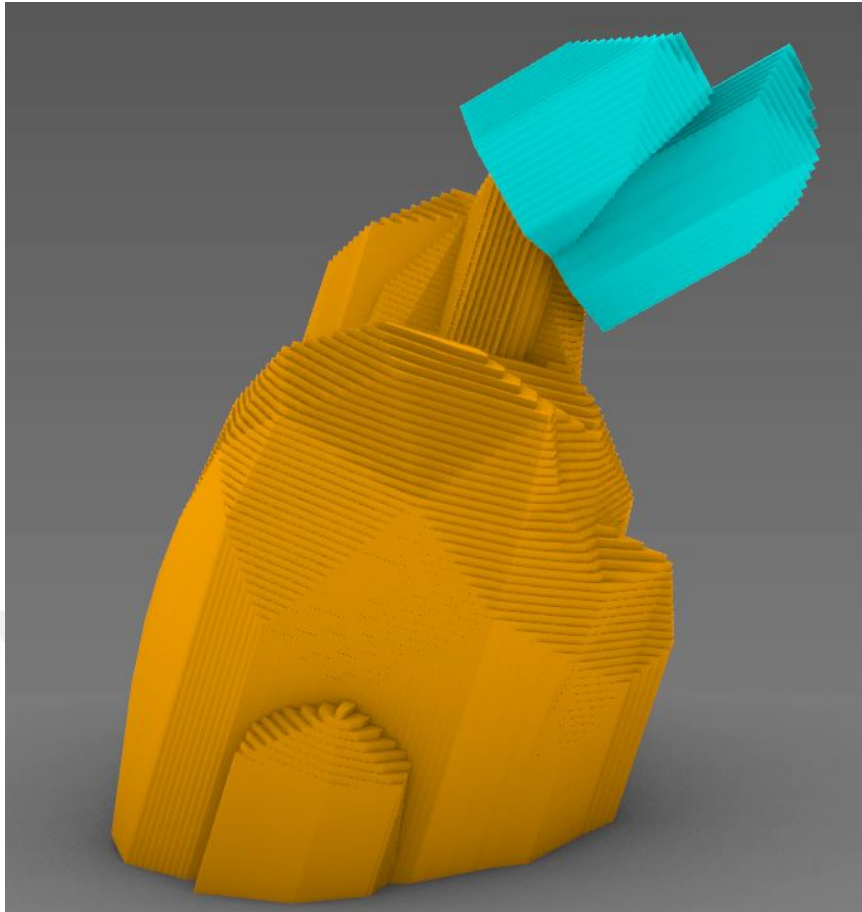


Figure 3.14: The Stanford Bunny, constructed with overhanging support volumes.

After a volume is projected to a lower plane, it also has to be connected to further layers, to prevent the overhang situation. In Figure 3.14, the ear part (cyan) of the Bunny is overhanging. Consequently, to handle this issue, the ears of the Bunny are firstly projected onto the lower tip side. Afterwards, this projection must be carried by an additional support volume, connecting the body of the Bunny with the ears. In the sample case, given in Figure 3.15, the overhanging ear volume is carried by green support volume.

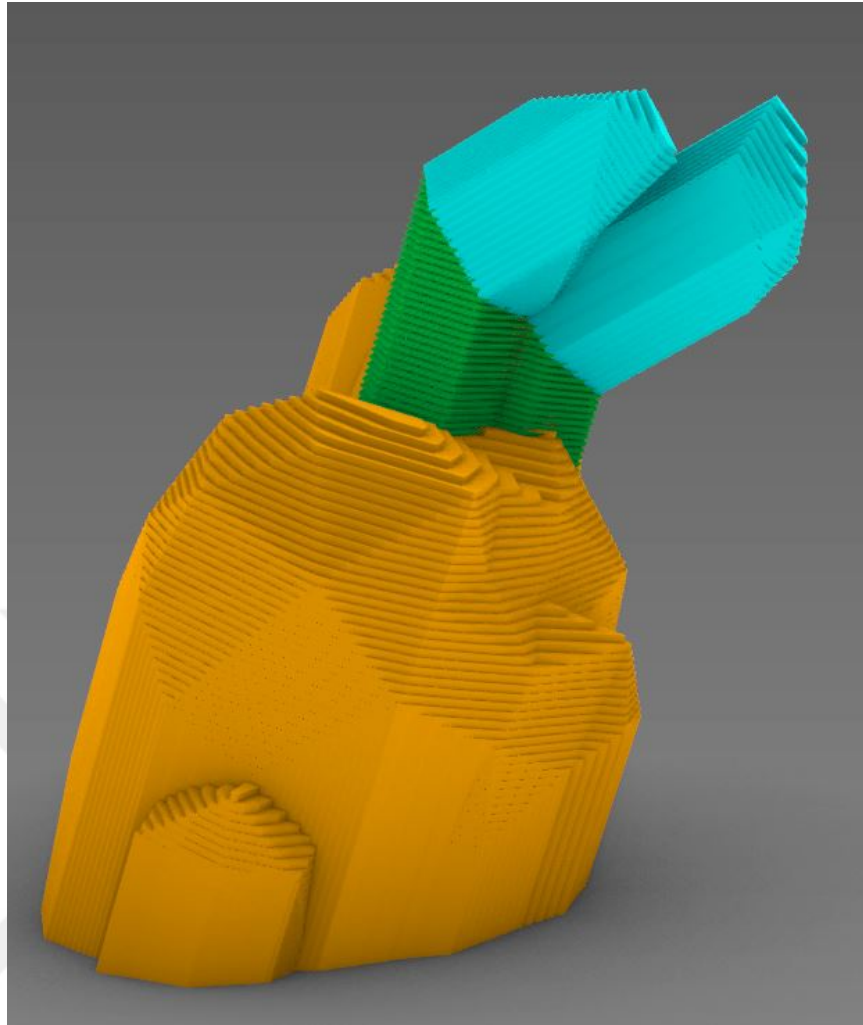


Figure 3.15: The green part is used to carry the cyan support volume.

The steps up to now are prepared for all the orientations. The product is examined and processed for the adaptive inclined slicing and their respective support requirements are derived. Grasshopper3D works way faster online processing in comparison with 3D volumetric processes. Consequently, the longer line length would result in higher support volume directly. Among all the options, the orientation with the least total line length is selected. The given sample orientations offer the least support material for  $5^\circ$  increments on the angular orientation.

### 3.6 Shell & Infill Patterns

In this section of the algorithm, the computations of the shell structures and infill patterns for both product and support structures are explained.

The boundary regions for each plane are obtained earlier in the Object Partitioning section. Using the shell parameters decided by the user in the input section, additional offset profiles are computed to represent the shell of the product.

After the computation of the shell, the infill volume can be found. As the infill pattern, parallel lines are used in the algorithm. The distance of these parallel lines,  $d_{line}$  has to be computed, with the inputs of the nozzle diameter,  $N_d$  and infill density,  $\rho_i$ .

Considering a 2D patterned rectangular region,  $N_d$  represents the thickness of these lines and  $\rho_i$  would be equal to the total proportion of material area to the inner cavity. With a simple derivation, Equation 3.2,  $d_{line}$  can be obtained. An example for the process is given in Figure 3.16.

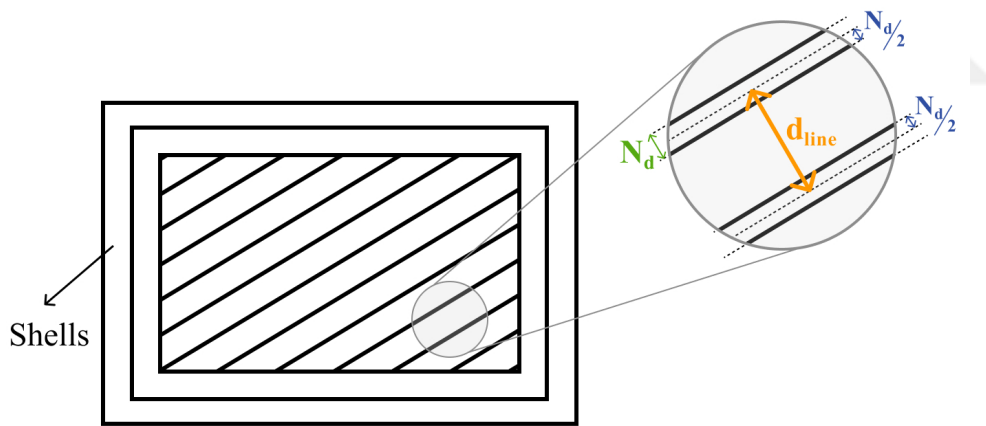


Figure 3.16: Representations of the nozzle diameter, shells & infill patterns.

$$\rho_i = \frac{N_d}{d_{line} + N_d} \quad (3.2)$$

Considering the Stanford Bunny, Figure 3.17 represents printing lines of a single layer. Here, the number of shells is taken as two, represented as green, with a relatively low dense infill. The infill printing lines are represented as red.

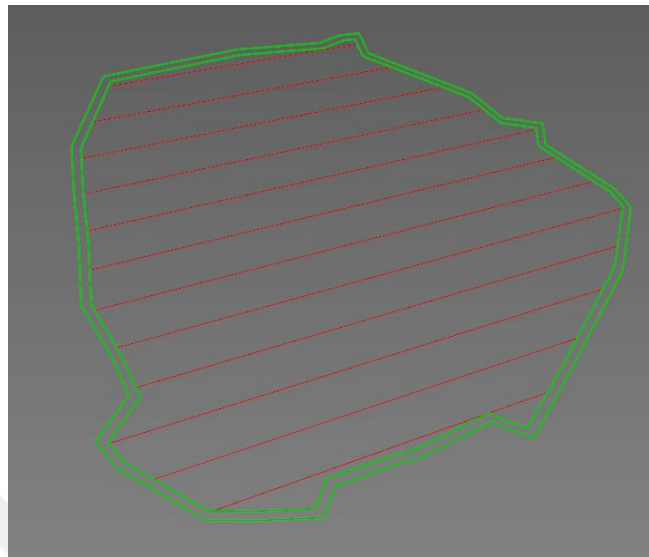


Figure 3.17: Representation of Nozzle Path, Shells & Infill, Single Layer

As an another illustration, Figure 3.18 is provided. Three different islands are sliced in a single plane, with the corresponding infills on a single layer. Simply, the nozzle will extrude, retract, continue to second island, retract again and complete the final zone.

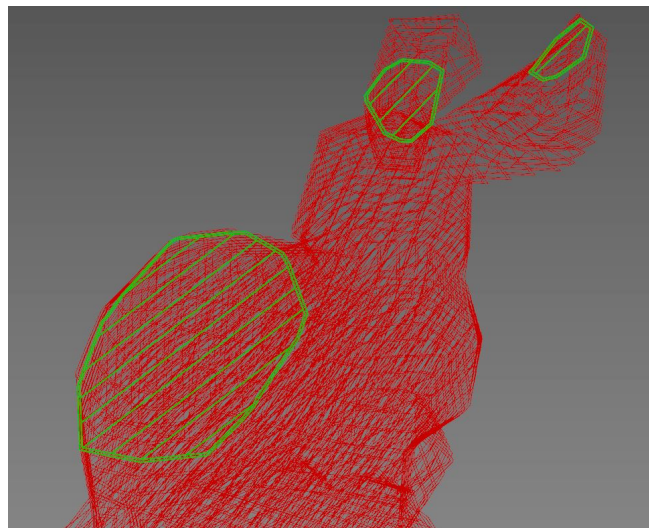


Figure 3.18: Representation of Nozzle Path, Shells & Infill, Single Layer, Islands

The same operation is repeated for the support volumes, with support infill ratio. The difference between the product's bounding region and the support region is calculated, and without shell structure, the support material is constructed.

With the conclusion of this part, the printing lines for adaptively the least support volume oriented product are derived. By using these printing lines, manufacturing data can be obtained as illustrated in Figure 3.19.

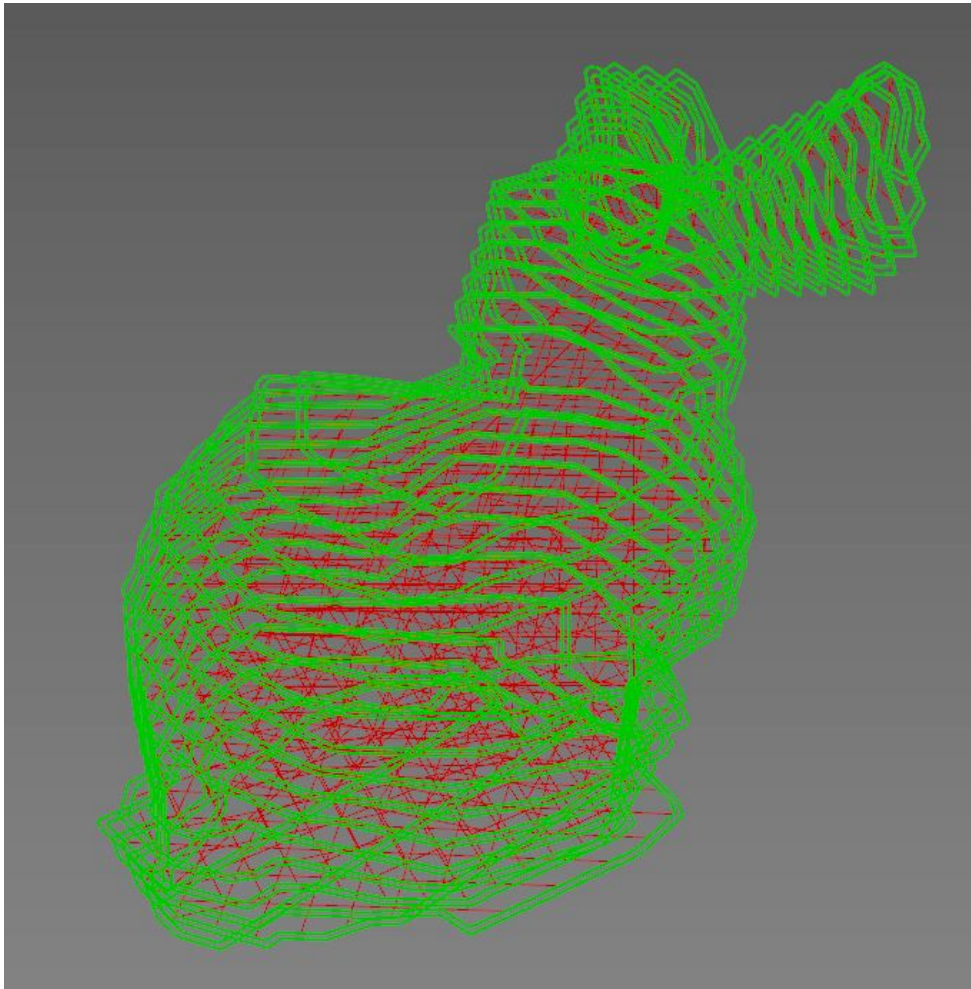


Figure 3.19: Representation of Nozzle Path, Shells & Infill, Complete Geometry

### 3.7 Manufacturing Data

Since the study case is different and is not applicable to the other type of 3D printers, computer-aided design and manufacturing processes have to be carried out by different algorithms. For this manner, the manufacturing data has to be evaluated.

In the classical FFF approach, manufacturing data is similar to the G-Code in the traditional machining operations. The process is adapted to this study. The movements and extruding process are evaluated by a GhPython script, using the printing lines as the input.

Considering the process, five elements are required to control the operation. Four of them are needed to control the movement and one is for controlling the extrusion process. These can be considered as follows.

- X-Axis Movement (mm)
- Y-Axis Movement (mm)
- Conveyor Belt Movement (mm)
- Inclination Angle (Degrees)
- Extrusion (Boolean / mm)

### 3.8 Sample Geometries

The algorithm is employed on two different geometries, the square collar and the hanger. Both require support structures once the conventional FFF 3D printing is used. For the first one, two slicing planes are enough to manufacture the product without any support structures using a 3D printer with a conveyor belt. The second example also requires two slicing plane, but this time the angle difference between the slicing planes is much higher than the first case.

#### 3.8.1 Square Collar

A square collar is provided as the first sample, given in Figure 3.20. There are holes on both sides and an inner square cavity in the product. It can be a critical component in an assembly. If the given orientation to be used in the conventional FFF 3D printers, then there should be support structures underneath the square cavity.

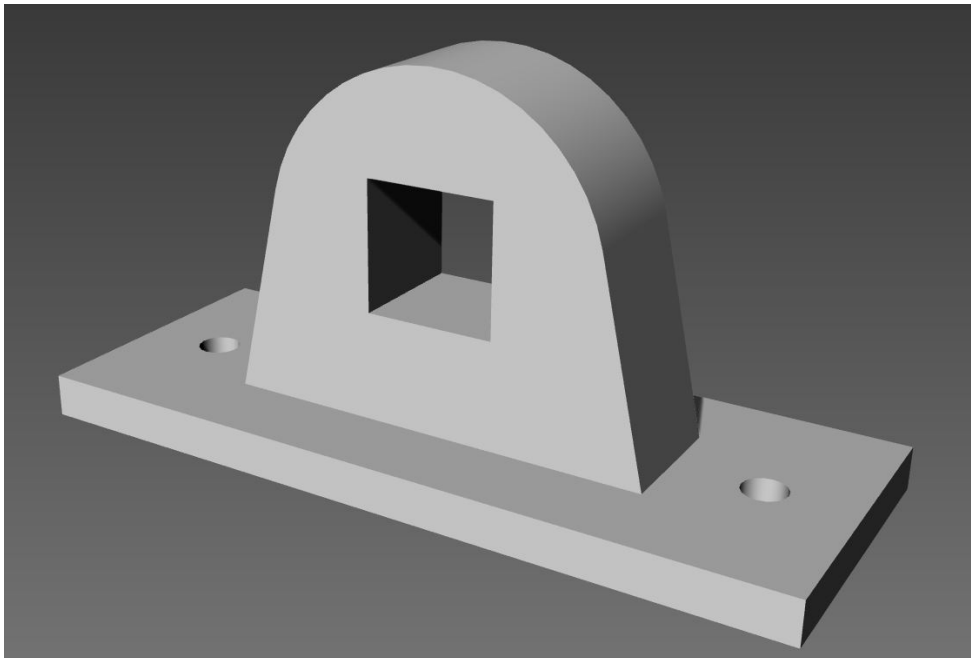


Figure 3.20: Square Collar

As given in Figures 3.21 and 3.22, the algorithm provides two printing planes. The first plane set is parallel to the initial printing plane, given as green, and the second plane is represented as red. The process starts from the left side of the geometry, and continues towards the second plane, with an inclination angle of  $5^\circ$ . The critical angle change occurs at the left tip corner of the square. At this point, inclination changes to  $45^\circ$ . The rest of the geometry is printed with respect to this plane. The square cavity would be manufactured without any support structures. Thus, the surface quality of the overall product would be much better than the case where support structures are utilized under the top surface of the cavity.

The rendered product is given in Figure 3.23. The red part of the square collar is printed with respect to the initial plane, and the orange part is printed with respect to the second plane. The support requirement of the inner square void is eliminated with the adaptive slicing and inclined 3D printing. In the manufacturing of this part, less material would be used and the process would be completed faster compared to the conventional 3D printing approach.

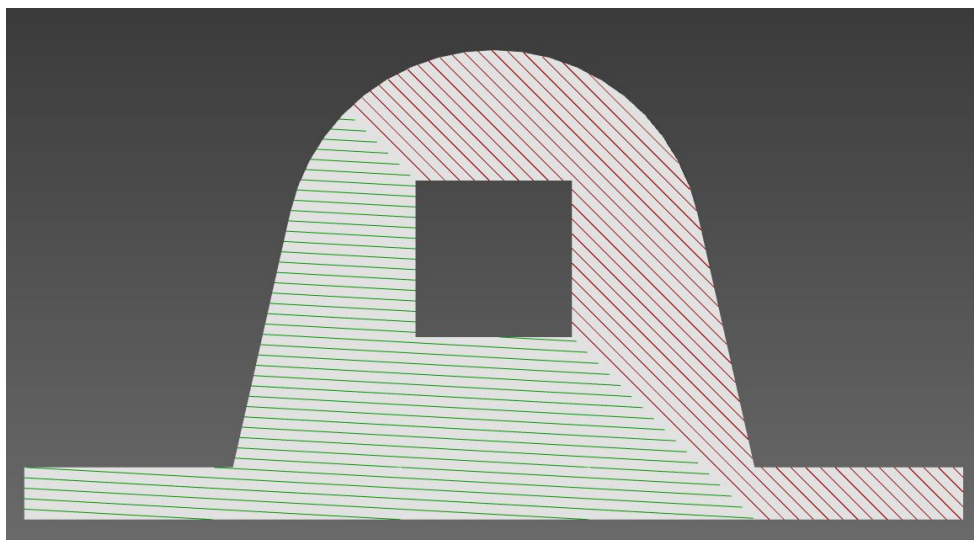


Figure 3.21: Square Collar Slicing, Normal View

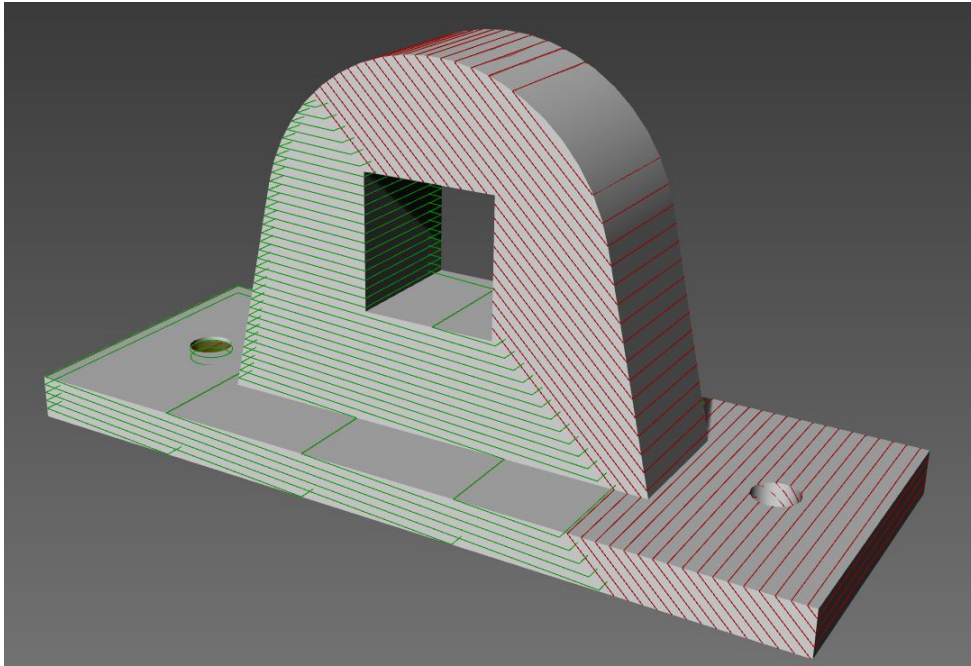


Figure 3.22: Square Collar Slicing, Perspective

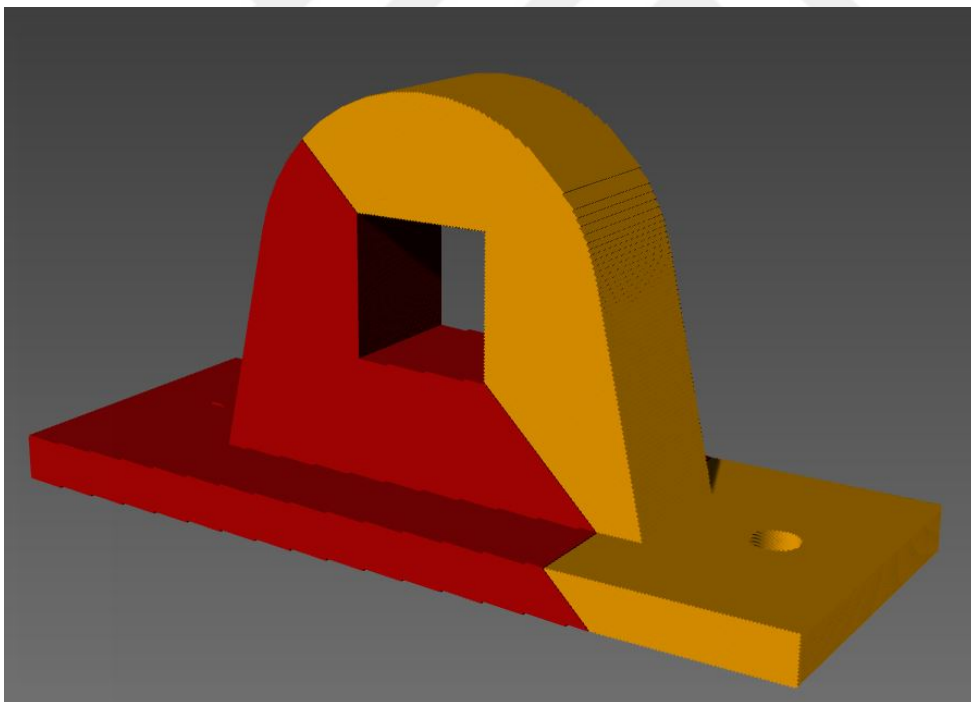


Figure 3.23: Square Collar, Rendered

### 3.8.2 Hanger

Another sample for the algorithm is a hanger, as shown in Figure 3.24. It has a cross section similar to a U-shape, which is a good example for the inclined 3D printing. If it is to be fabricated in this orientation using the standard 3D printers, it would require extensive amount of support structures. It may be fabricated in a different orientation, but then there needs to be support structures inside the hole.

As given in Figures 3.25 and 3.26, the algorithm provides two printing planes. The second plane divides the geometry into three different sub volumes. The process starts with the left side, with respect to the initial printing plane. Afterwards, the inclination angle changes at the tip point of the hanger, and separate the other into sub-volumes, which are extruded with respect to the second plane.

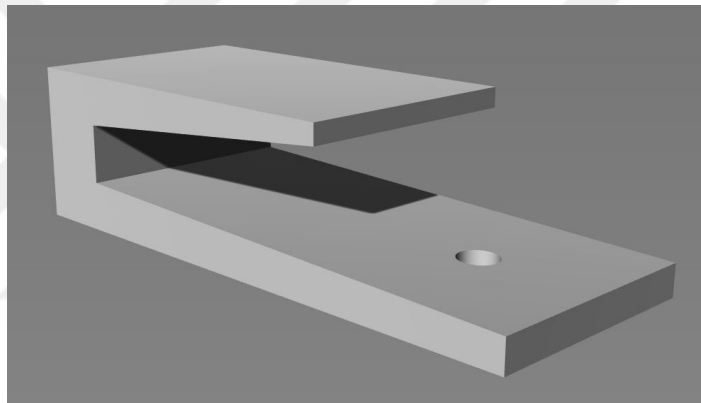


Figure 3.24: Hanger, Sample

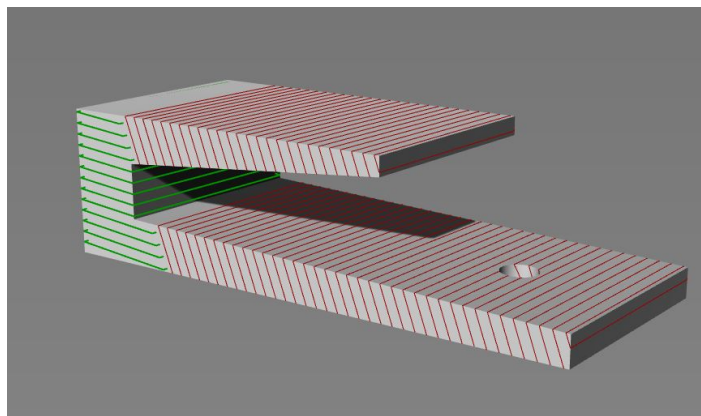


Figure 3.25: Hanger Slicing, Perspective

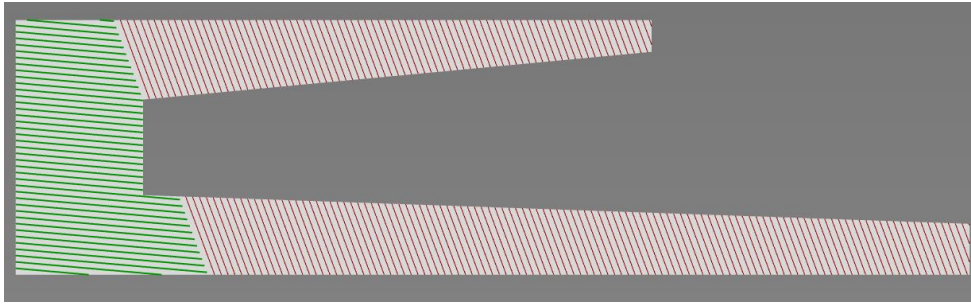


Figure 3.26: Hanger Slicing, Normal View

The rendered product is given as Figure 3.27. The blue part of the hanger is printed with respect to the initial plane, and the green parts are printed with respect to the second plane. These two sub volumes are printed and manufactured mutually. The support requirement due to the geometry of the hanger at this orientation is disabled with the adaptive slicing and inclined 3D printing.

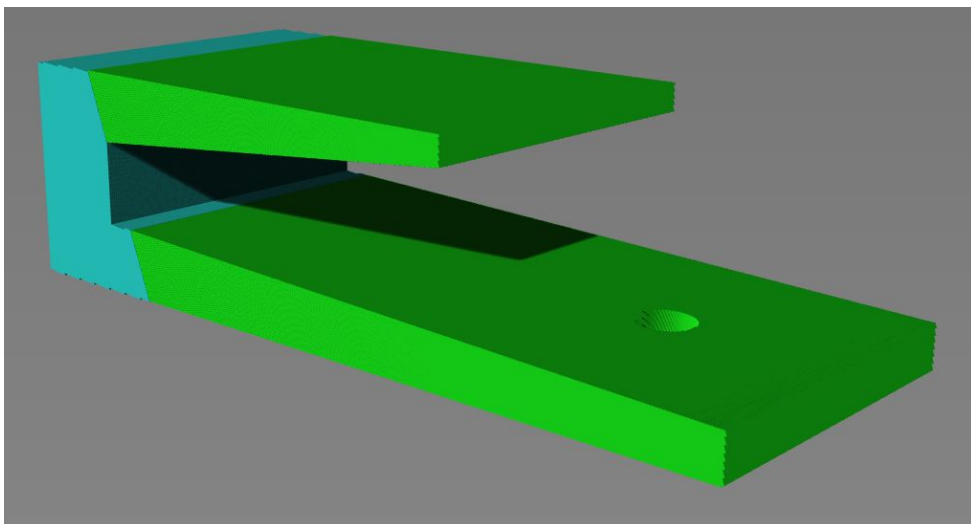


Figure 3.27: Hanger, Rendered

### 3.9 Time Complexity Analysis

Big-O Notation is used to define the time complexity of the adaptive inclined slicing algorithm. The Big-O Notation is used to classify the algorithm depending on its complexity.

Pseudocode of the algorithm is given earlier as Algorithm 3.1. It starts with the construction of an array which includes a number of orientations,  $O$ . The value directly depends on the input value, the number of iterations. At this point, an array of orientations is formed and stored. Afterwards, a parallel array is created with the derivation of outer profiles for each orientation and they are stored separately.

Following this, for each outer profile in the array, a set of operations start. The complexity depends on the initial geometry quality. On these oriented geometries and profiles, different operations are done throughout the algorithm, which are relatively not dominant in comparison with the orientations or the outer profile quality.

Considering the whole process, the algorithm has two nested loops in different intervals. Consequently, the Big-O Notation complexity of the system can be represented as  $O(mn)$ . Since  $n$  is referred as the more dominant factor, if the number of orientations is higher than the outer quality of the input geometry ( $m$ ),  $n$  would be the number of iterations, and becomes the main factor. On the contrary, if the overall mesh quality is higher and the number of iterations are relatively lower,  $n$  would be the overall geometry quality.

The worst case would be a high number of orientation iterations on a complex geometry. In that case, since both factors would be determinant, both of them may be referred as  $n$ , and the overall complexity level in the Big-O Notation would be  $O(n^2)$ .



## CHAPTER 4

### FABRICATION OF SAMPLE ARTIFACTS

#### 4.1 Introduction

In this chapter of the thesis, the fabrication process of the adaptive inclined 3D printer is explained. It starts with the required hardware for the realization of the approach. After brief information on the parts, the configuration, assembly and integration processes is given, the printing process is explained with some sample test prints.

#### 4.2 Hardware

For the adaptive inclined 3D printing, a conveyor belt system has to be combined with a nozzle, which is inclined and it may change its angle throughout the process. To handle this issue, a conveyor belt system is fixed to the printer bed of a multi-axis 3D printer, designed and produced earlier by Fazla et al. in the Mechanical Engineering Laboratory of Middle East Technical University [32]. The multi-axis 3D printer and its defined axes are given in Figure 4.1.

A conveyor belt system is designed, which has to be integrated into this system. It has to be fixed onto the print bed and the conveyor should be able to move without any obstacles. The rendered model of the conveyor belt is presented in Figure 4.2.

The assembly of the conveyor belt is given in Figure 4.3. The conveyor belt has a temperature-resistant belt, which has a rough surface in order to ease the adhesion of the extruded material to itself. The belt slides through two fixed cylinders on two shafts at the both ends.

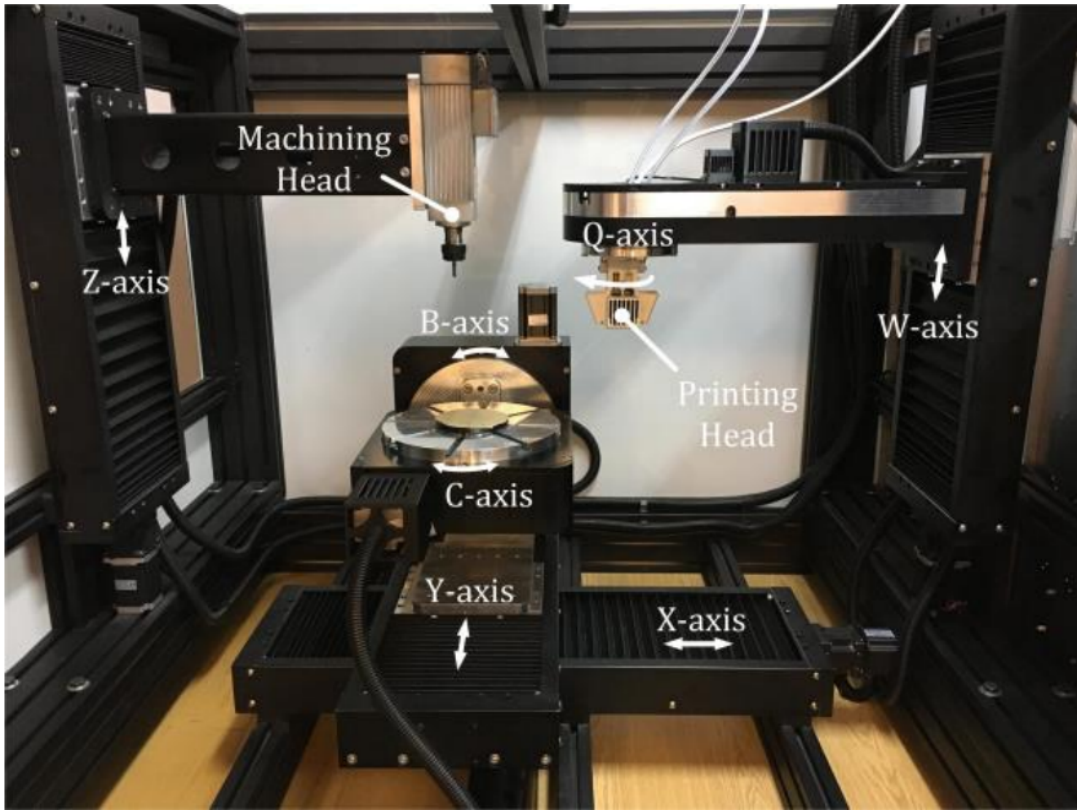


Figure 4.1: Multi-axis 3D printer [32]

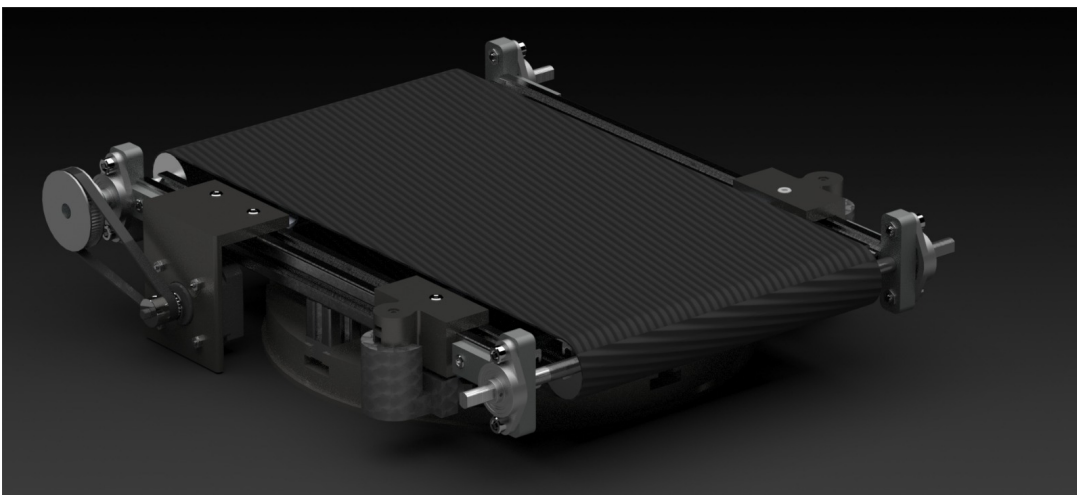


Figure 4.2: Conveyor Belt Model, Rendered



Figure 4.3: Conveyor belt

One of these shafts is connected to a stepper motor to control and actuate the system. Finally, there is a stretching rod, in order to eliminate any looseness on the belt. The rest of the system consists of mechanical connections, sigma profiles and supporting parts.

In Figure 4.4, the assembly is provided. A copper plate is placed for a better adhesion in the test prints, and a blue tape is placed for easier removal of the and re-usability of the plate.

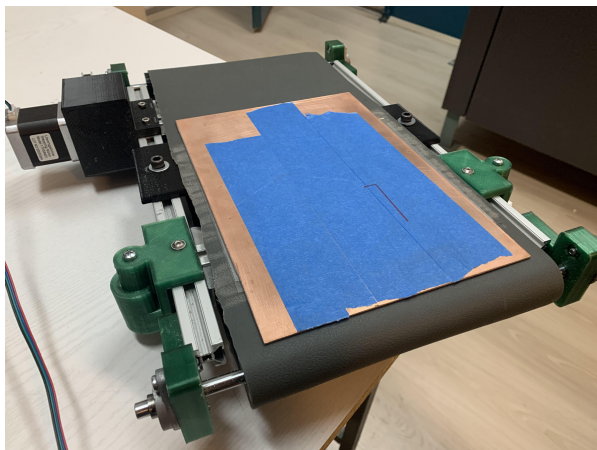


Figure 4.4: Conveyor belt assembly

### 4.3 Integration onto the Multi-axis Manufacturing System

By using two parallel supporting parts, the conveyor belt system is fixed to the manufacturing table of the multi-axis manufacturing system (HYBRO). Afterwards, the manufacturing data derived in the Chapter 3 is conveyed to the control system of the HYBRO.

As given in Figure 4.1, HYBRO has a control system for six different movement axes in the FFF process. However, considering the integration process, C-axis is disabled, since turning around Z-axis is not desired. X & Y-Axes are used in order to control the printing process for each layer. B-Axis is used to change the inclination angle and W-Axis is used to prevent the deviations since the rotation does not occur on the printing axis, but on the print bed where the conveyor belt is mounted. Finally, a new axis is defined in the system, referred as  $z_{belt}$ . It is a single directional axis which represents the movement of the belt provided by the stepper motor.

HYBRO has its own control system, and in order to integrate the conveyor belt the communication protocol is modified. Each point computed on the product must be transformed with respect to the nozzle's tip point. In addition, since the rotation axis is not at the tip of nozzle, the distance and coordinates must be transformed. For this manner, the following homogeneous transformation matrices are constructed.

${}^F T_x$  : Pose of Frame  $X$  with respect to Frame Fixed

${}^F T_X$  : Translate coordinates from Frame Fixed to Frame  $X$

$${}^F T_X = \begin{bmatrix} 1 & 0 & 0 & X \\ 0 & 1 & 0 & 0 \\ 0 & 0 & 1 & 0 \\ 0 & 0 & 0 & 1 \end{bmatrix} \quad (4.1)$$

$${}^xT_Y = \begin{bmatrix} 1 & 0 & 0 & 0 \\ 0 & 1 & 0 & Y \\ 0 & 0 & 1 & 0 \\ 0 & 0 & 0 & 1 \end{bmatrix} \quad (4.2)$$

$${}^Y T_B = \begin{bmatrix} \cos(\theta_B) & 0 & \sin(\theta_B) & 0 \\ 0 & 1 & 0 & 0 \\ -\sin(\theta_B) & 0 & \cos(\theta_B) & 0 \\ 0 & 0 & 0 & 1 \end{bmatrix} \quad (4.3)$$

$${}^B T_C = \begin{bmatrix} \cos(\theta_C) & -\sin(\theta_C) & 0 & 0 \\ \sin(\theta_C) & \cos(\theta_C) & 0 & 0 \\ 0 & 0 & 1 & c_{BC} \\ 0 & 0 & 0 & 1 \end{bmatrix} \quad (4.4)$$

$${}^C T_{\text{Belt}} = \begin{bmatrix} 1 & 0 & 0 & x_{\text{Belt}} \\ 0 & 1 & 0 & 0 \\ 0 & 0 & 1 & c_{\text{belt}} \\ 0 & 0 & 0 & 1 \end{bmatrix} \quad (4.5)$$

$${}^{\text{Belt}} T_P = \begin{bmatrix} 1 & 0 & 0 & a_P \\ 0 & 1 & 0 & b_P \\ 0 & 0 & 1 & c_P \\ 0 & 0 & 0 & 1 \end{bmatrix} \quad (4.6)$$

$${}^F T_{\text{AM}} = \begin{bmatrix} 1 & 0 & 0 & 0 \\ 0 & 1 & 0 & 0 \\ 0 & 0 & 1 & W + c_{\text{FAM}} \\ 0 & 0 & 0 & 1 \end{bmatrix} \quad (4.7)$$

The annotations on the matrices refer as follows.

- $c_{BC}$ : constant offset between B-axis and C-axis along Z
- $c_{belt}$ : constant offset between C-axis and Belt-axis along Z (thickness of the Belt-platform)
- $c_{FAM}$ : constant offset between C-axis and Belt-axis along Z (thickness of the Belt-platform)
- $X$ : Motion command on X axis
- $Y$ : Motion command on Y axis
- $W$ : Motion command on AM axis
- $x_{Belt}$ : Motion command on the Belt axis, assumed to be in the global X direction (since  $C=0$  will be used)
- $a_P$ : constant offset of the workpiece with respect to the Belt-fixed axis along X (generally 0)
- $b_P$ : constant offset of the workpiece with respect to the Belt-fixed axis along Y (generally 0)
- $c_P$ : constant offset of the workpiece with respect to the Belt-fixed axis along Z (some offset may be added in order to avoid collision)

After multiplications,

$${}^{AM}T_P = {}^{AM}T_F {}^F T_X {}^X T_Y {}^Y T_B {}^B T_C {}^C T_{Belt} {}^{Belt} T_P \quad (4.8)$$

$${}^{AM}T_P = \begin{bmatrix} \cos(\theta_B) \cos(\theta_C) & -\cos(\theta_B) \sin(\theta_C) & \sin(\theta_B) & K \\ \sin(\theta_C) & \cos(\theta_C) & 0 & L \\ -\sin(\theta_B) \cos(\theta_C) & \sin(\theta_B) \sin(\theta_C) & \cos(\theta_B) & M - (W + c_{FAM}) \\ 0 & 0 & 0 & 1 \end{bmatrix} \quad (4.9)$$

where:

$$K = X + (a_P + x_{\text{Belt}}) \cos(\theta_B) \cos(\theta_C) - b_P \cos(\theta_B) \sin(\theta_C) + (c_{BC} + c_P + c_{\text{belt}}) \sin(\theta_B) \quad (4.10)$$

$$L = Y + (a_P + x_{\text{Belt}}) \sin(\theta_C) + b_P \cos(\theta_C) \quad (4.11)$$

$$(4.12)$$

$$M = -(a_P + x_{\text{Belt}}) \sin(\theta_B) \cos(\theta_C) + b_P \sin(\theta_B) \sin(\theta_C) + (c_{BC} + c_P + c_{\text{belt}}) \cos(\theta_B) \quad (4.13)$$

As mentioned earlier, all of the points should be transformed to the origin of the nozzle.

$${}^P \text{Points} = \begin{bmatrix} pn_x \\ pn_y \\ pn_z \end{bmatrix} \quad (4.14)$$

$${}^{AM} \text{Points} = {}^{AM} T_P {}^P \text{Points} \quad (4.15)$$

$$\begin{bmatrix} 0 \\ 0 \\ 0 \\ 1 \end{bmatrix} = D \begin{bmatrix} pn_x \\ pn_y \\ pn_z \\ 1 \end{bmatrix} \quad (4.16)$$

where D is:

$$D = \begin{bmatrix} \cos(\theta_B) \cos(\theta_C) & -\cos(\theta_B) \sin(\theta_C) & \sin(\theta_B) & K \\ \sin(\theta_C) & \cos(\theta_C) & 0 & L \\ -\sin(\theta_B) \cos(\theta_C) & \sin(\theta_B) \sin(\theta_C) & \cos(\theta_B) & M - (W + c_{\text{FAM}}) \\ 0 & 0 & 0 & 1 \end{bmatrix} \quad (4.17)$$

After the multiplications, X-Y and W can be derived as

$$X = - \left( (pn_x + x_{belt} + a_P) \cos(\theta_B) \cos(\theta_C) - (pn_y + b_P) \cos(\theta_B) \sin(\theta_C) \right. \\ \left. + (pn_z + c_{BC} + c_P + c_{belt}) \sin(\theta_B) \right) \quad (4.18)$$

$$Y = - \left( (pn_x + x_{belt} + a_P) \sin(\theta_C) + (pn_y + b_P) \cos(\theta_C) \right) \quad (4.19)$$

$$W = - \left( (pn_x + x_{belt} + a_P) \sin(\theta_B) \cos(\theta_C) + (pn_y + b_P) \sin(\theta_B) \sin(\theta_C) \right. \\ \left. + (pn_z + c_{BC} + c_P + c_{belt}) \cos(\theta_B) - c_{FAM} \right) \quad (4.20)$$

The final unknown to set is  $x_{belt}$ , representing the movement of the conveyor belt. Considering our approach, C-axis rotation will always be zero. Thus, the belt motion will be in the direction of X-axis.

B-axis rotation is selected with respect to the slicing angle. Slicing angle is the angle between the Z-axis and the normal of a slice. For instance, if the slicing angle is  $45^\circ$ , normal vector becomes (0.707,0.0,0.707).

Since the AM-axis is stationary, W will always be constant. Thus, the last equation only allows B-axis rotation and belt motion commands. Since the B-axis rotation is fixed, required belt motion can be calculated by the last equation. After setting  $C = 0$ , the equation becomes

$$x_{belt} = \frac{- (pn_x + a_P) \sin(\theta_B) + (pn_z + c_{BC} + c_P + c_{belt}) \cos(\theta_B) - c_{FAM} - W}{\sin(\theta_B)} \quad (4.21)$$

To conclude, the integration values are derived by the Grasshopper3D, processed and sent to the conveyor belt & HYBRO assembly throughout the process.

## 4.4 Test Prints

In this chapter, the test prints on the Conveyor Belt & HYBRO Assembly are elaborated. In the ideal case for the inclination approach, the nozzle would directly extrude to the tip of the conveyor belt. However, in this case, the distance between the nozzle's tip and nozzle's base is so small to sustain better control on heat. It is not possible to extrude material directly onto the conveyor belt since the nozzle would collide with the belt assembly. Thus, a base copper plate is fixed to the conveyor belt and a base material is connected to this plate to avoid any possible collisions. Alternative approaches and results are presented and discussed throughout this section.

### 4.4.1 Sample 1 - Single Angle

In this first print, a basic hanger model is prepared. Angle change and retraction are disabled to observe the initial setup and the printing results. The printing angle is set to  $39.8^\circ$ . The setup and the process is given in Figure 4.5, and the resulting product is provided in Figures 4.6-4.8.

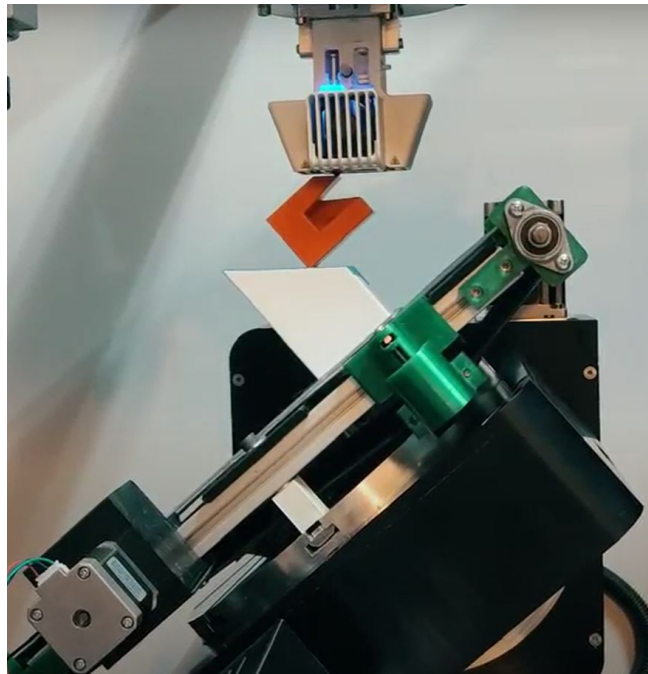


Figure 4.5: Setup for Sample 1

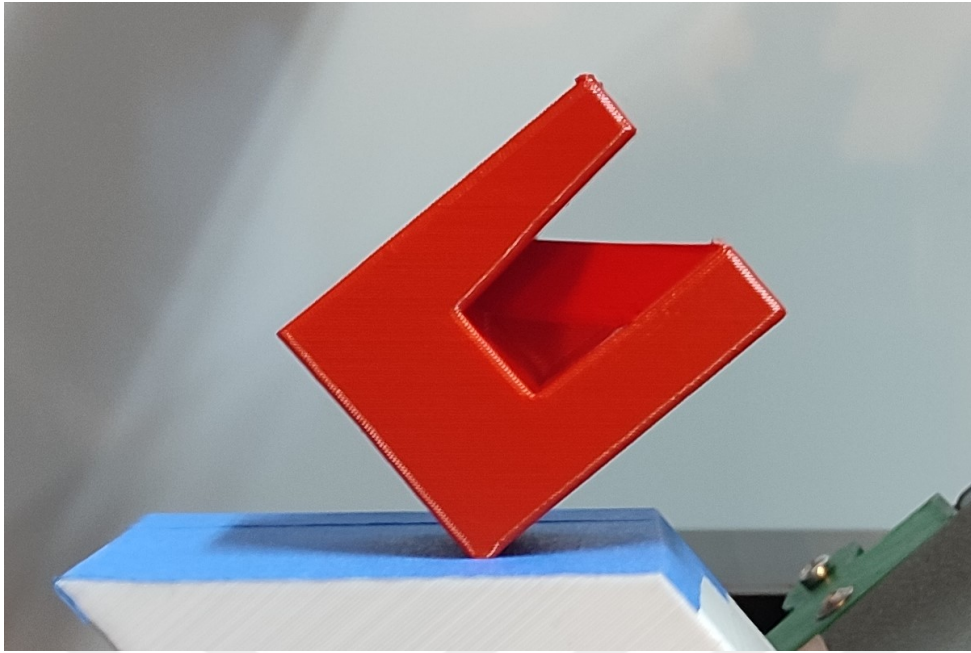


Figure 4.6: Sample 1

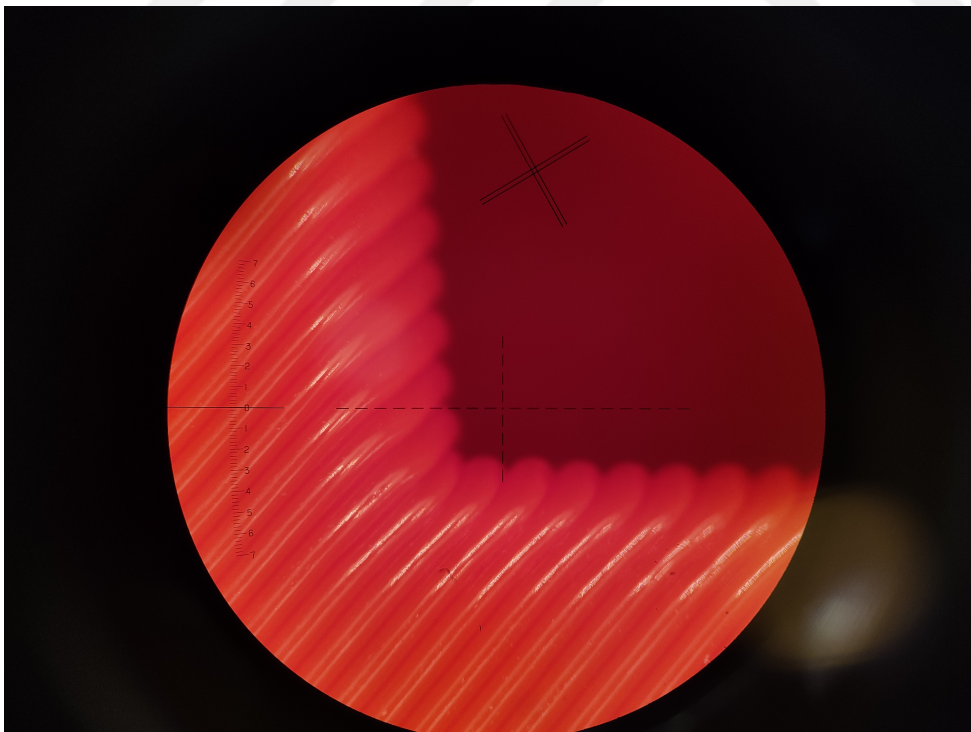


Figure 4.7: Sample 1, Layers

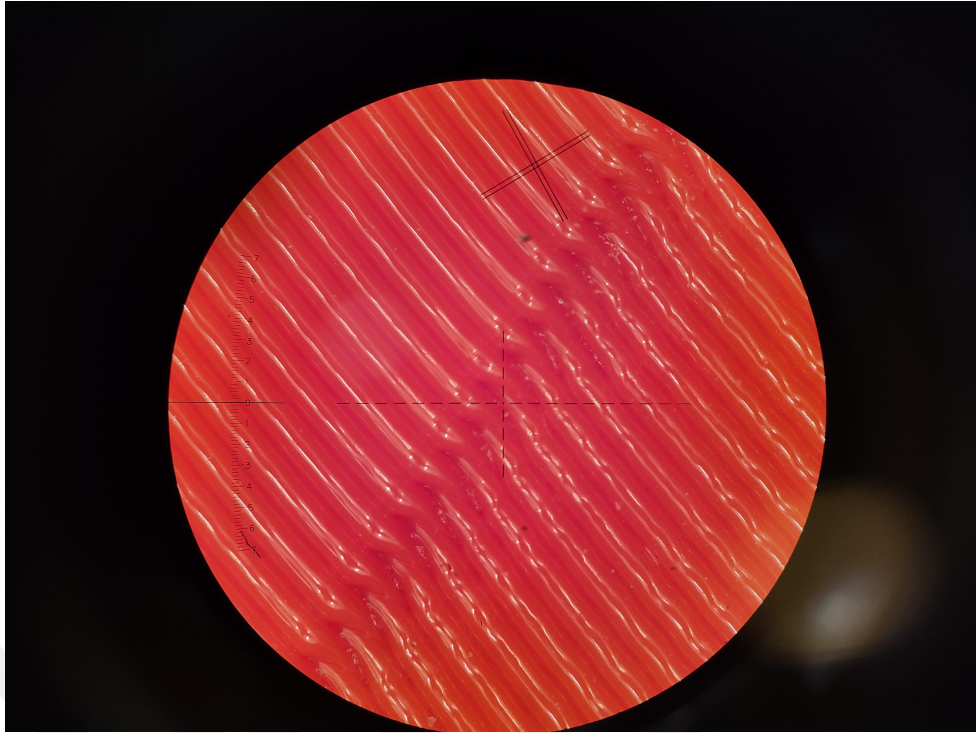


Figure 4.8: Sample 1, Layers, Seam Zone

#### 4.4.2 Sample 2 - Double Angle

In the second print, the same workpiece is studied, with an inclination change. Similar to the first sample, the initial angle is set to  $39.8^\circ$ , and after the critical point, it is changed to  $62.2^\circ$ . Red coloured filament is used for the primary part, and it is followed with grey, as can be seen in Figures 4.9-4.13. Following them, the zoomed views of the product are given as Figures. The matching zone layers are collapsed as desired.

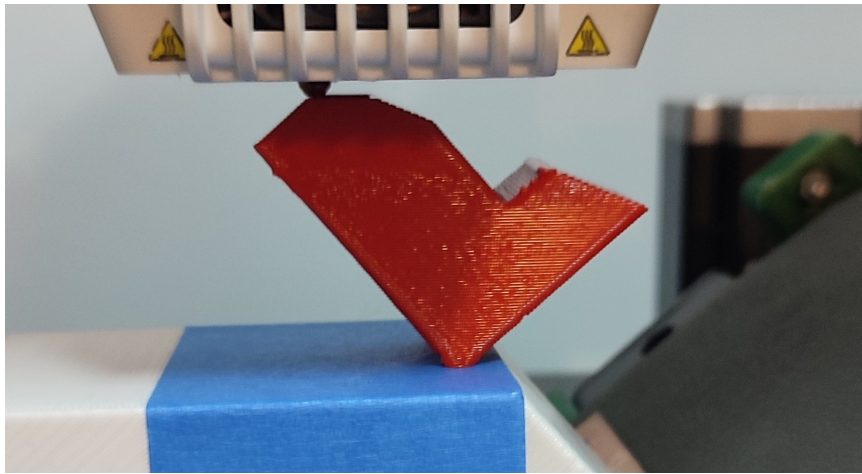


Figure 4.9: Sample 2, Initial Part

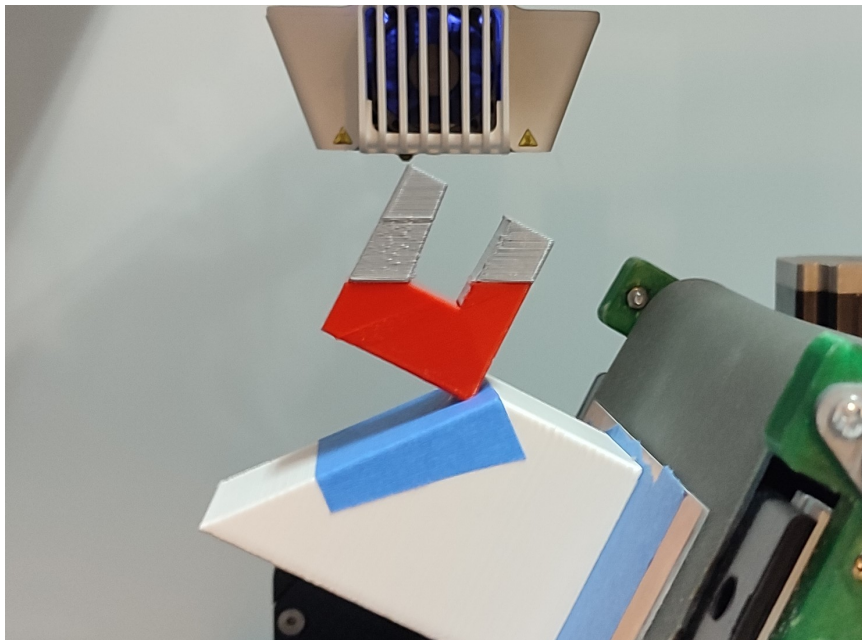


Figure 4.10: Sample 2, Final Product

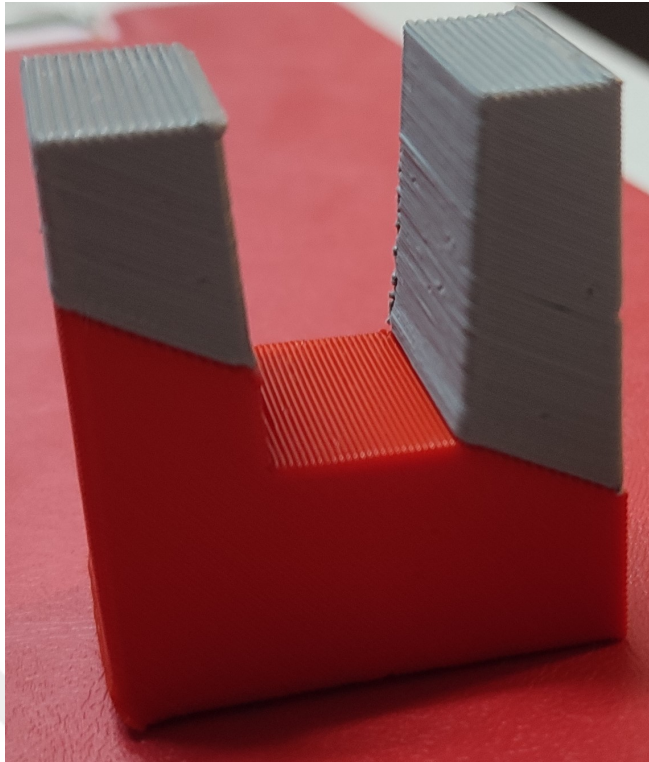


Figure 4.11: Sample 2, Final Product

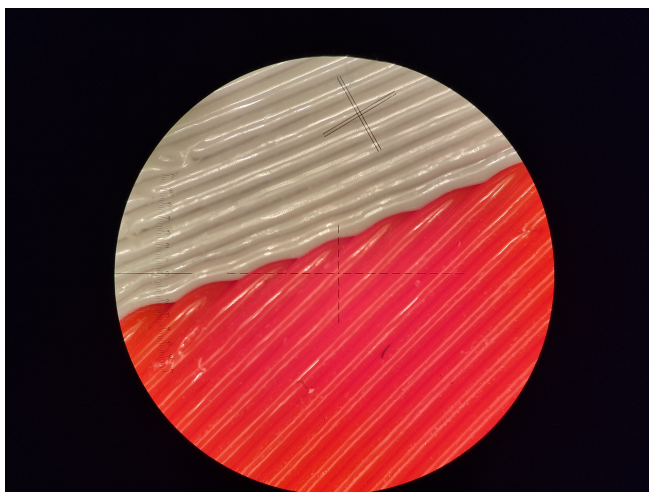


Figure 4.12: Sample 2, Layers, Inclination Change Zone

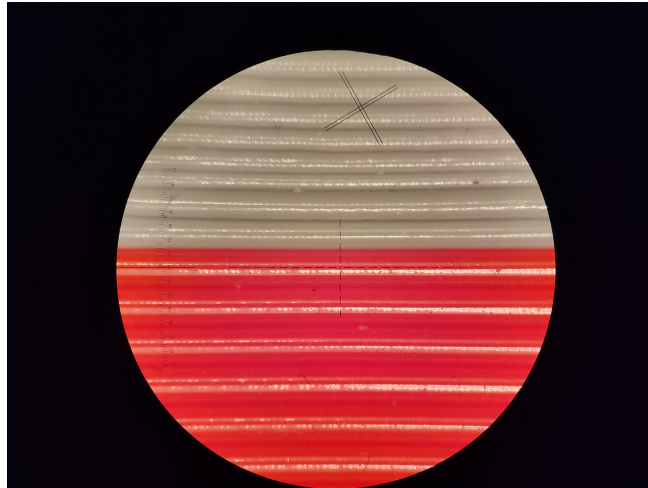


Figure 4.13: Sample 2, Layers, Inclination Change Zone, Side View for Parallel Lines

In this sample, retraction is enabled. While moving between islands, there is a major retraction effect on the overall quality of the workpiece. The start of the layers with islands is similar to the first sample, just providing a seam zone. However, when the nozzle moves from one island to the other, there occurs a quality reduction at the start of second island due to the discontinuous movement, as shown in Figures 4.14-4.15.

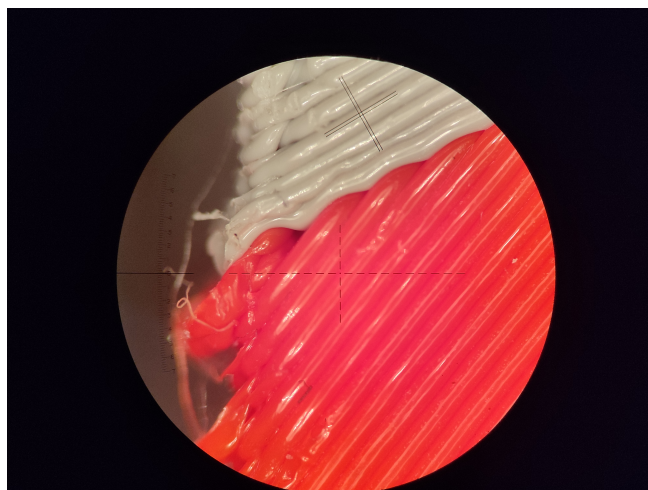


Figure 4.14: Sample 2, Layers, Retraction Effect

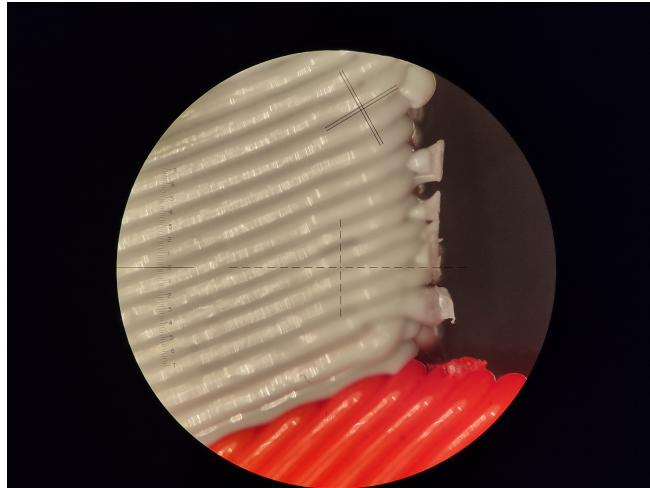


Figure 4.15: Sample 2, Layers, Retraction Effect

#### 4.4.3 Sample 3 - Triple Angles

In this final print, the part is extended for a double angle change, starting with  $39.8^\circ$ , continues with  $62.2^\circ$  and finally, by the last breaking point, it moves back to the initial position,  $39.8^\circ$ . The part printed using initial angle is coloured grey, connecting second part is coloured red and the part with final angle is coloured black.

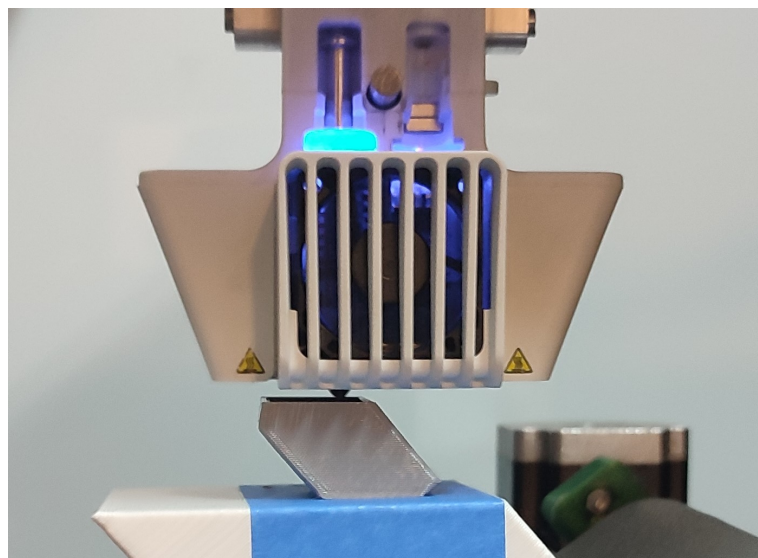


Figure 4.16: Sample 3, Grey Part

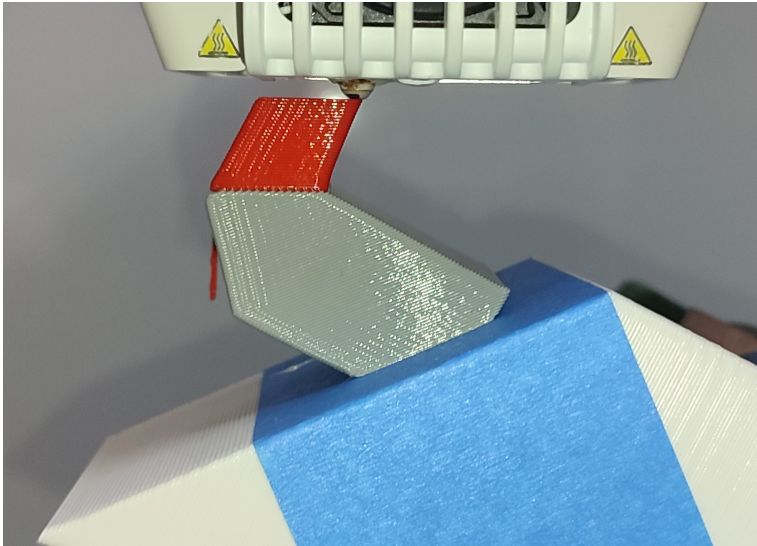


Figure 4.17: Sample 3, Red Part

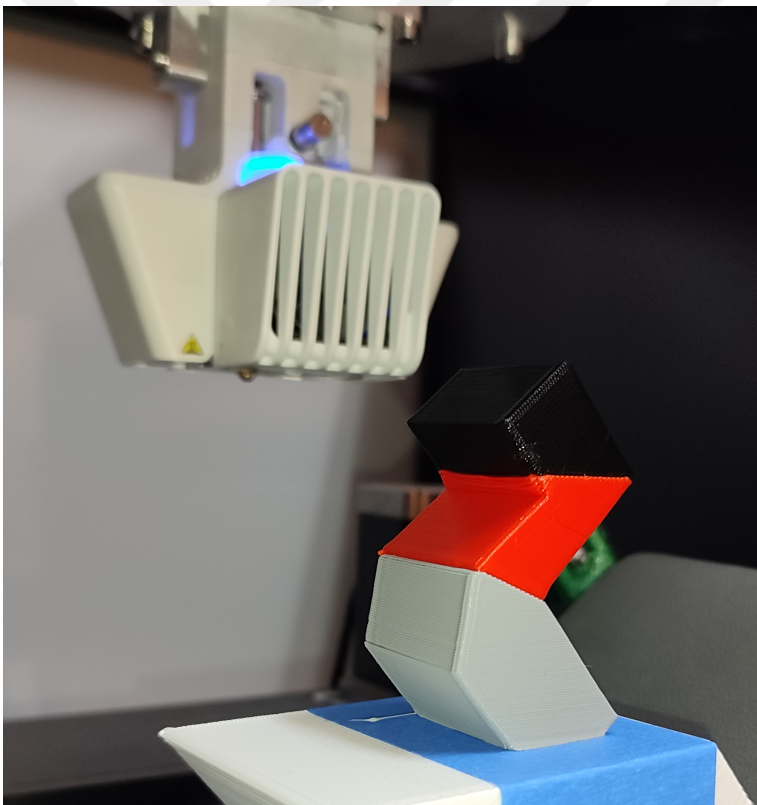


Figure 4.18: Sample 3, Final Product

Since there aren't any islands on this final product, the quality reduction due to the retraction in the second sample doesn't occur. The layers of the product are shown in Figures 4.19 and 4.20.

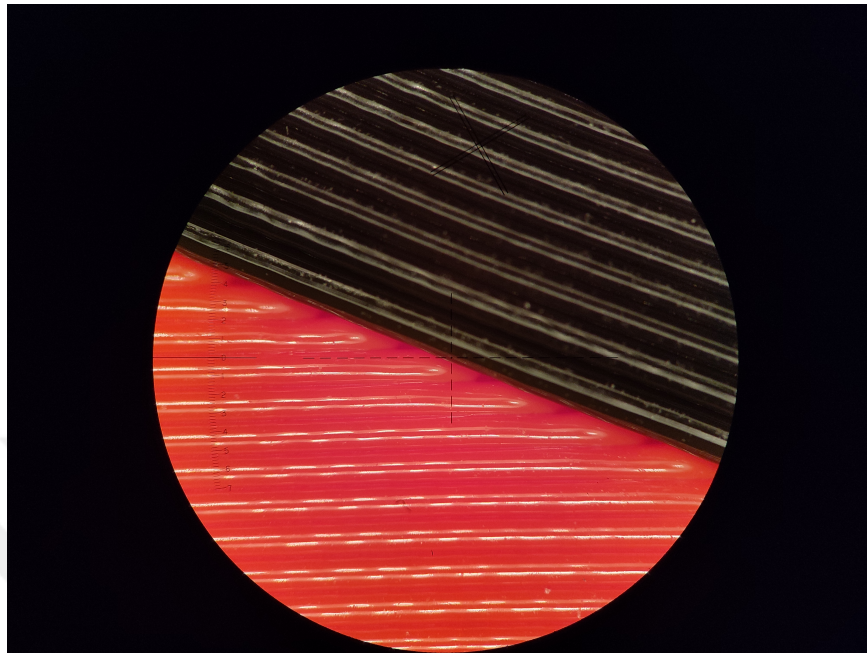


Figure 4.19: Sample 3, Layers, Black & Red Zones

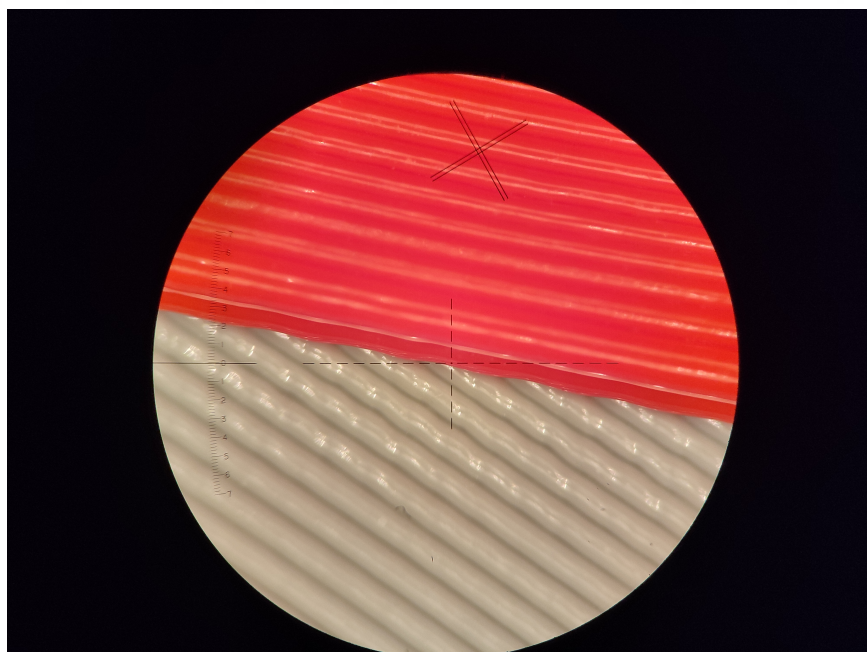


Figure 4.20: Sample 3, Layers, Red & Grey Zones



## CHAPTER 5

### CONCLUSIONS

In this thesis, an adaptive inclined slicing algorithm is integrated into a FFF 3D printer with an inclined conveyor belt. After introducing the scope and contributions of the thesis, brief background information is provided throughout Chapter 2. AM and the FFF process are introduced with samples from the literature, and the earlier studies on support minimization & mass production are presented. Following this, in Chapter 3, the adaptive inclined slicing algorithm is explained. Data structure, steps of the algorithm and the optimization process are described by using flowcharts and sample geometries. In Chapter 4, the production and integration process are presented, with some sample test prints.

In the literature, there are many research, methods and strategies based on support material minimization. Most of them are applied in different operations to improve the manufacturing process. On the other hand, application of conveyor belts, which provides users an infinite 3D printing volume and mass manufacturing capabilities, is not a common approach. With the adaptive inclined 3D printing, it is aimed to bring a new geometry-dependent responsive strategy. While enabling the conveyor belt benefits, by making the process adaptive, the support optimization is applied via adjusting the inclination angle.

The studied algorithm can provide the respective geometry-dependent slicing layers, while finding the optimum orientation for the minimum amount of support structures. An iterative approach is used directly since there can't be an optimized strategy covering any type of geometry. With higher number of iteration set as input, efficient printing angles can be obtained.

Regarding the integration on the HYBRO manufacturing system, output data with coordinates, printing angles and retractions are generated. Afterwards, with the given matrices in Chapter 4, the data is converted to the HYBRO's syntax.

Following this, during the test prints, it is observed that the adaptive printing process improves the overall process considering time and material. With the support optimization and adaptive slicing, requirement for support material is reduced, as well as the time for printing of the respective volume is prevented. In addition, the overall process time is further improved considering the separation of support structures from the product.

The products are presented with detailed views. On the inclination change zones, the process goes as desired. In the end of the primary part, a base plane is constructed for the upcoming part in the respective angle. Although the smoothness of the initial layer is not as good as the traditional 3D printing, the jagged structure does not cause any problem for the upcoming inclined layer. However, when the retraction is enabled for the islands, there is a quality reduction at the start of the second island. As a future study, retraction settings can be optimized for better surface quality.

Another future work could be implementing the setup to a system similar to the conveyor belt 3D printers such as Blackbelt3D or Creality CR30. HYBRO system and the nozzle height restricts movements since this setup was not designed for belt 3D printing. Especially with a longer nozzle, whose temperature control is also optimized for this manner, the movements can be made in an easier way and complex trajectories can be processed.

## REFERENCES

- [1] C. Achillas, D. Tzetzis, and M. O. Raimondo, “Alternative production strategies based on the comparison of additive and traditional manufacturing technologies,” *International Journal of Production Research*, vol. 55, no. 12, pp. 3497–3509, 2017.
- [2] T. Pereira, J. V. Kennedy, and J. Potgieter, “A comparison of traditional manufacturing vs additive manufacturing, the best method for the job,” *Procedia Manufacturing*, vol. 30, pp. 11–18, 2019. Digital Manufacturing Transforming Industry Towards Sustainable Growth.
- [3] A. Jimo, C. Braziotis, H. Rogers, and K. Pawar, “Traditional vs additive manufacturing supply chain configurations: A comparative case study,” *Procedia Manufacturing*, vol. 39, pp. 765–774, 2019. 25th International Conference on Production Research Manufacturing Innovation: Cyber Physical Manufacturing August 9-14, 2019 | Chicago, Illinois (USA).
- [4] B. Westerweel, R. J. Basten, and G.-J. van Houtum, “Traditional or additive manufacturing? assessing component design options through lifecycle cost analysis,” *European Journal of Operational Research*, vol. 270, no. 2, pp. 570–585, 2018.
- [5] S. S. Crump, “Apparatus and method for creating three-dimensional objects,” Jun 1992.
- [6] “What is fdm (fused deposition modeling) 3d printing? explained by hubs.”
- [7] “What are supports in 3d printing? when and why do you need them? | hubs 2022.”
- [8] *Sustainability of 3D Printing: A Critical Review and Recommendations*, vol. Volume 2: Materials; Biomanufacturing; Properties, Applications and Sys-

tems; Sustainable Manufacturing of *International Manufacturing Science and Engineering Conference*, 06 2016. V002T05A004.

- [9] E. Karasik, R. Fattal, and M. Werman, “Object partitioning for support-free 3d-printing,” *Computer Graphics Forum*, vol. 38, no. 2, pp. 305–316, 2019.
- [10] J. Lipina, V. Krys, and J. Sedlák, “Shaped glued connection of two parts made by rapid prototyping technology,” vol. 555, pp. 541–548, 2014.
- [11] M. K. Wlodarczyk-Biegun, J. Paez, M. Villiou, and A. del Campo, “Medical adhesives for 3d printing,” 2017.
- [12] Z. Wang, P. Song, and M. Pauly, “State of the art on computational design of assemblies with rigid parts,” in *Computer graphics forum*, vol. 40, pp. 633–657, Wiley Online Library, 2021.
- [13] H. ming Zhao, Y. He, J. zhong Fu, and J. jiang Qiu, “Inclined layer printing for fused deposition modeling without assisted supporting structure,” *Robotics and Computer-Integrated Manufacturing*, vol. 51, pp. 1–13, 2018.
- [14] Z. Zhu, S. Keimasi, N. Anwer, L. Mathieu, and L. Qiao, “Review of shape deviation modeling for additive manufacturing,” in *Advances on Mechanics, Design Engineering and Manufacturing*, pp. 241–250, Springer, 2017.
- [15] K. Hu, S. Jin, and C. C. Wang, “Support slimming for single material based additive manufacturing,” *Computer-Aided Design*, vol. 65, pp. 1–10, 2015.
- [16] Y.-H. Kuo, C.-C. Cheng, Y.-S. Lin, and C.-H. San, “Support structure design in additive manufacturing based on topology optimization,” *Structural and Multi-disciplinary Optimization*, vol. 57, no. 1, pp. 183–195, 2018.
- [17] J. Jiang, X. Xu, and J. Stringer, “Optimization of process planning for reducing material waste in extrusion based additive manufacturing,” *Robotics and Computer-Integrated Manufacturing*, vol. 59, pp. 317–325, 2019.
- [18] C. Dai, C. C. Wang, C. Wu, S. Lefebvre, G. Fang, and Y.-J. Liu, “Support-free volume printing by multi-axis motion,” *ACM Transactions on Graphics (TOG)*, vol. 37, no. 4, pp. 1–14, 2018.

- [19] W. De Backer, A. P. Bergs, and M. J. Van Tooren, "Multi-axis multi-material fused filament fabrication with continuous fiber reinforcement," in *2018 AIAA/ASCE/AHS/ASC Structures, Structural Dynamics, and Materials Conference*, p. 0091, 2018.
- [20] M. K. Thompson, G. Moroni, T. Vaneker, G. Fadel, R. I. Campbell, I. Gibson, A. Bernard, J. Schulz, P. Graf, B. Ahuja, *et al.*, "Design for additive manufacturing: Trends, opportunities, considerations, and constraints," *CIRP annals*, vol. 65, no. 2, pp. 737–760, 2016.
- [21] Z. Doubrovski, J. C. Verlinden, and J. M. Geraedts, "Optimal design for additive manufacturing: opportunities and challenges," in *International design engineering technical conferences and computers and information in engineering conference*, vol. 54860, pp. 635–646, 2011.
- [22] A. Wiberg, J. Persson, and J. Ölvander, "Design for additive manufacturing—a review of available design methods and software," *Rapid Prototyping Journal*, 2019.
- [23] E. Recrosio, "Understand units and sizes for your 3d printing dimensions," 2016.
- [24] J. Jiang, X. Xu, and J. Stringer, "Optimisation of multi-part production in additive manufacturing for reducing support waste," *Virtual and Physical Prototyping*, vol. 14, no. 3, pp. 219–228, 2019.
- [25] M. Vélez, E. Toala, and J. C. Zagal, "Koala 3d: A continuous climbing 3d printer," *Robotics and Computer-Integrated Manufacturing*, vol. 64, p. 101950, 2020.
- [26] X. Zhang, M. Li, J. H. Lim, Y. Weng, Y. W. D. Tay, H. Pham, and Q.-C. Pham, "Large-scale 3d printing by a team of mobile robots," *Automation in Construction*, vol. 95, pp. 98–106, 2018.
- [27] D. O'Connor, "Blackbelt 3d - what we know," 2017.
- [28] K. Sertoglu, "Creality launches its 3dprintmill (cr-30) conveyor belt 3d printer on kickstarter - 3d printing industry," 2022.

- [29] D. H. Dam, H. N. Le, D. T. Bui, and N. L. Nguyen, “A research on conveyor belt 3d printer in industrial applications,” 2019.
- [30] D. Günther, B. Heymel, J. F. Günther, and I. Ederer, “Continuous 3d-printing for additive manufacturing,” *Rapid Prototyping Journal*, 2014.
- [31] G. Turk and M. Levoy, “Zippered polygon meshes from range images,” in *Proceedings of the 21st annual conference on Computer graphics and interactive techniques*, pp. 311–318, 1994.
- [32] B. Fazla, M. U. Dilberoğlu, U. Yaman, and M. Dölen, “Multi-axis 3d printing of spiral parts without support structures,” *Journal of Additive Manufacturing Technologies*, vol. 1, no. 2, pp. 558–558, 2021.



## APPENDIX A

### GHPYTHON SCRIPTS

The GHPython Scripts used for slicing angle derivation and manufacturing data generation in the algorithm are provided in this chapter.

#### A.1 Slicing Angle Derivation

---

```
1  """Provides a scripting component.
2      Inputs:
3          x: Outward Normal List
4          y: Initial Layer
5          z: Exploded Point List
6          u: Initial Point
7          v: Critical Angle
8      Output:
9          h: Plane List"""
10
11  import rhinoscriptsyntax as rs
12
13  a=list() #pointlist
14  if rs.VectorAngle([0,0,1],y)>=90:
15      y=rs.VectorReverse(y)
16  new=y
17  i=0
18  c=list()
19  h=list()
20  c.append(rs.PlaneFromNormal(z[u+1],y))
21  h.append(c[0])
22  x.pop(u)
23  z.pop(u)
24  e=list()
25  f=list()
26
27  i=len(x)-1
28  while i>0:
```

```

29     if x[i].X>0 and x[i].Z<0 :
30         direct=rs.VectorRotate(x[i],90,rs.CreateVector(0,-1,0))
31         print(rs.VectorAngle(new,direct))
32         if rs.VectorAngle(new,direct)>v and
33         rs.VectorAngle(x[i],rs.CreateVector(0,0,1))>(180-v):
34             a.append(z[i+1])
35             f.append(rs.PlaneFromNormal(z[i+1],
36             rs.VectorUnitize(rs.VectorAdd(direct,new))))
37             h.append(rs.PlaneFromNormal(z[i+1],
38             rs.VectorUnitize(rs.VectorAdd(direct,new))))
39             e.append(rs.AddLine(z[i],z[i+1]))
40             print(rs.VectorAngle(new,direct))
41             direct=rs.VectorUnitize(direct)
42             new=rs.VectorUnitize(rs.VectorAdd(direct,new))
43             if rs.VectorAngle([0,0,1],new)>=90:
44                 new=rs.VectorReverse(new)
45         i-=1

```

---

## A.2 Manufacturing Data Generation

```

1  """Provides a scripting component.
2  Inputs:
3      x: Point
4  Output:
5      a: Manufacturing Code"""
6
7  import rhinoscriptsyntax as rs
8
9
10 d=float(x.X)
11 e=float(x.Y)
12 f=float(x.Z)
13
14 a=( str(d) + " " + str(e) + " " + str(f) + " " + str(y))

```

---

```

1  """Provides a scripting component.
2  Inputs:
3      x: Manufacturing Data
4      y: Retraction Indices
5  Output:
6      a: Manufacturing Data List"""
7
8  import rhinoscriptsyntax as rs
9
10 i=0

```

```
11 a=x
12 while i<len(x):
13     if i in y:
14         a[i]=a[i]+" 0"
15     else:
16         a[i]=a[i]+" 1"
17     i+=1
```

---

